



# PACIFIC EARTHQUAKE ENGINEERING RESEARCH CENTER

## **Characterization of Large Velocity Pulses for Laboratory Testing**

**Kenneth E. Cox**

University of California, San Diego

**and**

**Scott A. Ashford**

University of California, San Diego

# **Characterization of Large Velocity Pulses for Laboratory Testing**

**Kenneth E. Cox**

Department of Structural Engineering  
University of California, San Diego

and

**Scott A. Ashford**

Department of Structural Engineering  
University of California, San Diego

Final report on research supported primarily by the  
Earthquake Engineering Research Centers Program of the  
National Science Foundation under award number  
EEC-9701568

PEER Report 2002/22  
Pacific Earthquake Engineering Research Center  
College of Engineering  
University of California, Berkeley  
April 2002

## **ABSTRACT**

The occurrence of a greater than magnitude 6 earthquake in an urban setting is a rare event; however, structural performance during such an earthquake is an important consideration. Unique to the near-fault region (less than 10 km) is the occurrence of a large pulse in the velocity time history trace. This large velocity pulse occurs when the conditions of forward directivity are met.

The ability to capture pulse-type ground motions in the near-fault region is of recent development and records of this type are few. The 1994 Northridge, California, and 1995 Kobe, Japan, earthquakes substantially increased the current database of recorded ground motions. As technologies improve and seismic recording devices become less expensive and easier to implement, the database of recorded near-fault directivity pulses will increase. For example, numerous devices in the near-fault region captured the recent (1999) Kocaeli, Turkey, and Chi-Chi, Taiwan, earthquakes. The effect of this recent data on previously completed work is discussed.

Correct modeling and design of structures subjected to near-fault, directivity pulse loading require a sound understanding of the pulse characteristics of near-fault motions. This report describes the procedure followed in defining a representative large velocity pulse for laboratory testing. The laboratory testing was sponsored by the Pacific Earthquake Engineering Research Center, University of California, Berkeley. Included in the discussion is an analysis of the factors affecting pulse characteristics.

## **ACKNOWLEDGMENTS**

This work was supported in part by the Pacific Earthquake Engineering Research Center through the Earthquake Engineering Research Centers Program of the National Science Foundation under award number ECC-9701568.

# CONTENTS

<b>ABSTRACT</b> .....	<b>iii</b>
<b>ACKNOWLEDGMENTS</b> .....	<b>iv</b>
<b>TABLE OF CONTENTS</b> .....	<b>v</b>
<b>LIST OF FIGURES</b> .....	<b>vii</b>
<b>LIST OF TABLES</b> .....	<b>ix</b>
<b>1 INTRODUCTION</b> .....	<b>1</b>
1.1 Directivity Pulses .....	1
1.2 Laboratory Testing at UCSD .....	2
1.3 Pulse Characterization.....	5
<b>2 BACKGROUND</b> .....	<b>7</b>
2.1 Directivity Effects .....	7
2.2 Implications for Engineered Structures.....	11
2.3 Availability of Near-Fault Records.....	13
<b>3 DATA COLLECTION</b> .....	<b>15</b>
3.1 Description of Records.....	15
3.2 Pulse Recognition .....	20
3.3 Rotation to Fault Normal .....	21
3.4 Typical Pulse.....	24
3.5 Attenuation Relations.....	26
<b>4 DEVELOPMENT OF THE MEAN PULSE</b> .....	<b>31</b>
4.1 Extraction of the Directivity Pulses .....	31
4.2 Normalization of Pulse Records.....	33
4.3 Construction of the Mean Pulse .....	34
<b>5 CHARACTERIZATION OF THE LOADING PROTOCOL</b> .....	<b>37</b>
5.1 Response of the Prototype Column.....	37
5.2 Response of the Prototype Joint.....	44
<b>6 THE KOCAELI AND CHI-CHI EARTHQUAKES</b> .....	<b>49</b>

<b>7</b>	<b>SUMMARY AND CONCLUSIONS.....</b>	<b>57</b>
	<b>REFERENCES.....</b>	<b>59</b>

## LIST OF FIGURES

Figure 1.1	Column test specimen .....	3
Figure 1.2	Beam and column joint rebar assembly .....	4
Figure 2.1	Directivity refers to the direction of rupture propagation .....	8
Figure 2.2	Defining a site as forward, reverse or neutral directivity .....	9
Figure 2.3	Effect of accumulation of seismic energy (after Abrahamson, 1998).....	10
Figure 2.4	The large velocity pulse occurs in the fault-normal direction (after Somerville, 1993).....	11
Figure 2.5	Sylmar Olive View Medical Center .....	12
Figure 3.1	Velocity particle trace from the Rinaldi Receiving Station, Northridge earthquake .....	18
Figure 3.2	Velocity squared time history for the Rinaldi Receiving Station, Northridge earthquake.....	21
Figure 3.3	Acceleration in the fault-normal direction when the accelerometers are oriented north and east .....	22
Figure 3.4	Acceleration in the fault-normal direction when the accelerometers are orthogonal.....	23
Figure 3.5	Recorded Accelerations A and B result from the absolute acceleration vector, C .....	24
Figure 3.6	Period of the pulse predicted by $r$ . Data are normalized to $M_w = 7$ .....	27
Figure 3.7	Period of the pulse predicted by $M_w$ . Data are normalized to $r = 5$ km .....	28
Figure 3.8	Peak velocity predicted by $\phi$ . Data are normalized to $M_w = 7$ .....	29
Figure 3.9	Peak velocity predicted by $M_w$ . Data are normalized to $\phi = 15^\circ$ .....	29
Figure 4.1	All records found to contain a pulse. The pulse is in bold .....	32
Figure 4.2	Comparison of all catalogued pulses and the mean pulse.....	33
Figure 4.3	Mean large velocity pulse scaled to the average peak velocity value .....	35
Figure 5.1	Analytical response of the column to the mean large velocity pulse .....	40
Figure 5.2	Simplified analytical column response time history .....	41
Figure 5.3	Simplified analytical column response scaled by 22% .....	42
Figure 5.4	Displacement time history for the first test .....	43
Figure 5.5	Displacement time history for the third test .....	44
Figure 5.6	Loading protocol for the beam-column joint tests .....	47

Figure 6.1	Kocaeli and Chi-Chi records found to contain a pulse. The pulse is in bold. ....	51
Figure 6.2	Isolated pulses and the mean pulse .....	52
Figure 6.3	Mean pulse including the data from Kocaeli and Chi-Chi.....	52
Figure 6.4	Period of the pulse predicted by $M_w$ . Data are normalized to $\phi = 15^\circ$ .....	54
Figure 6.5	Period of the pulse predicted by $\phi$ . Data are normalized to $M_w = 7$ .....	54
Figure 6.6	Peak velocity predicted by $r$ . Data are normalized to $\phi = 15^\circ$ .....	55
Figure 6.7	Peak velocity predicted by $\phi$ . Data are normalized to $r = 5$ km .....	55

## LIST OF TABLES

Table 3.1	All records analyzed for the presence of a pulse.....	17
Table 3.2	Records containing pulses.....	25
Table 3.3	Correlation values for period and peak velocity .....	27
Table 5.1	Properties of the prototype column .....	38
Table 5.2	Properties of the single-degree-of-freedom model.....	38
Table 5.3	Response of the single-degree-of-freedom column .....	39
Table 5.4	Simplified column response values.....	40
Table 5.5	Simplified column response values scaled by 22% .....	41
Table 5.6	Column prototype properties for the joint specimens .....	44
Table 5.7	Pile prototype properties for the joint specimens.....	45
Table 5.8	Column properties for Ruaumoko.....	45
Table 5.9	Pile properties for Ruaumoko .....	46
Table 6.1	Kocaeli and Chi-Chi records containing pulses .....	50
Table 6.2	Correlation values for period and peak velocity .....	53

# 1 Introduction

Near-fault records differ from more common seismic records in several significant ways. If the conditions of forward directivity are satisfied, the record will be shorter in duration, higher in frequency content, and the majority of the seismic energy will be delivered in a large velocity pulse. These near-fault effects were first noticed in the 1971 San Fernando, California, earthquake and serious concern was raised following the 1994 Northridge, California, and 1995 Hyogo-ken Nanbu (Kobe), Japan, earthquakes. Section 2.2 will discuss the implications of these velocity pulses on engineered structures. The objective of this report is to characterize directivity large velocity pulses for the intent of modeling the pulse in structural testing. Details of the structural testing carried out based on this model will only be briefly discussed, although additional information can be found elsewhere (Gibson, 2001; Makley, 2001; Orozco, 2001).

## 1.1 DIRECTIVITY PULSES

The occurrence of large earthquakes that produce near-fault effects under an urban setting is unavoidable. Since the 1971 San Fernando earthquake, engineers and seismologists have studied the effects of near-source ground motions on buildings. The 1994 Northridge earthquake and the 1995 Kobe earthquake provided new information about the behavior of engineered structures within close proximity to the rupture zone. These near-fault effects result in ground shaking that subjects the structure to loading that was not represented in the design codes. Structural engineers first studied the near-fault effects on buildings and implemented design factors in the 1997 Uniform Building Code (UBC). Bridge engineers have begun to investigate the effects of near-fault motions on bridges.

Perhaps the most important characteristic of near-fault records is the occurrence of a large velocity pulse resulting from directivity effects. Pulses can also be found in the

acceleration and displacement traces of many near-fault records; however, the velocity pulse appears to be more important from an engineering standpoint. The velocity pulse coupled with a large peak displacement during the pulse gives rise to considerable damage potential (Hall et al., 1995). A large displacement without the high velocity pulse does not have a significant damaging potential because the structure is able to respond and follow the ground.

## **1.2 LABORATORY TESTING AT UCSD**

The testing for which the pulse characterization was required was sponsored by the Pacific Earthquake Engineering Research (PEER) Center. To gain a better understanding of the requirements of the pulse characterization and loading protocol thence derived, a brief description of the testing program follows.

PEER conducted a study to investigate the effects of near-fault large velocity pulses on bridge piers. The study was a multi-university collaborative effort which involved the University of California at San Diego (UCSD), Berkeley (UCB), and Irvine (UCI), the University of Southern California (USC), and the California Institute of Technology (Caltech). UCB conducted a shake table test with a mass on top of a column. UCSD, UCI, and USC performed further testing under varying loading protocols to develop a suite of comparable information. Caltech performed analytical studies of the effects of velocity pulses.

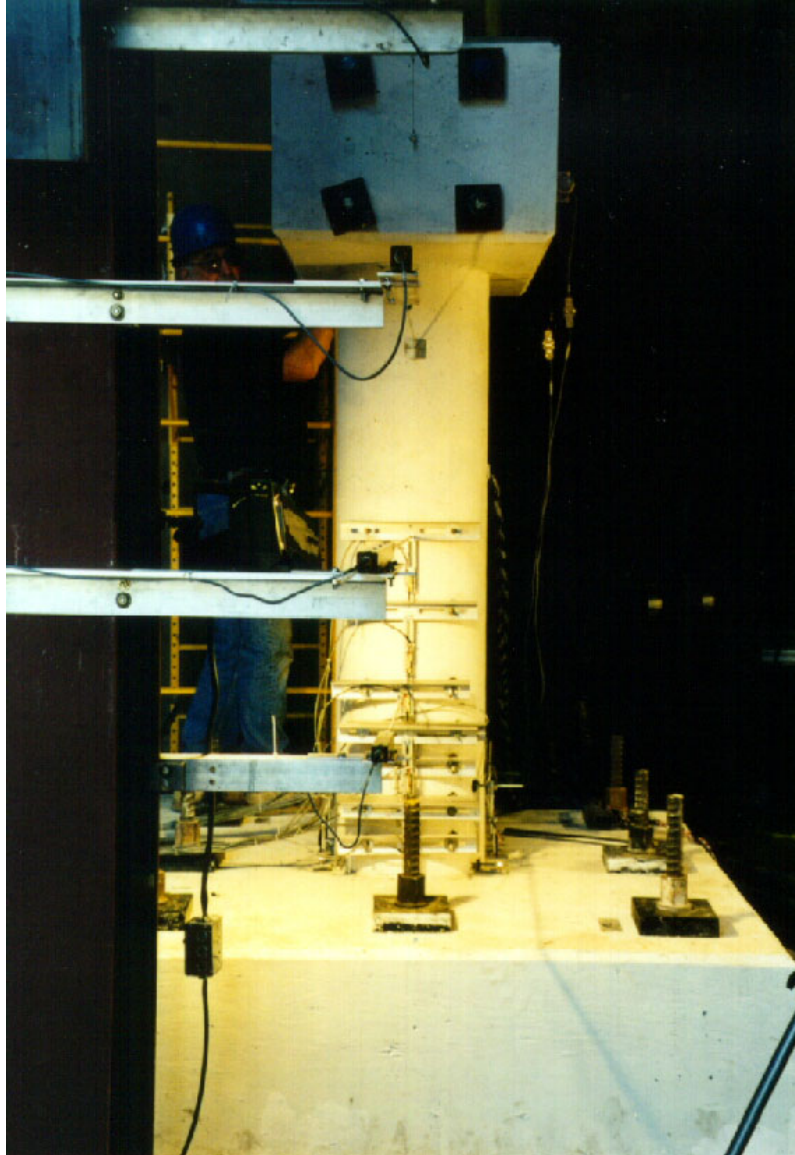


**Fig. 1.1 Column test specimen**

At UCSD, three circular bridge columns at 22% scale were tested in the Charles Lee Powell Structural Systems Research Laboratories under loading protocol containing a large velocity pulse. The design of each of the columns was identical. Figure 1.1 is a photograph of one of these column specimens as it was set up in the lab. Each column was subjected to the same sequence of peak displacements under varying loading rates.

UCSD also tested four bridge T-joints connections at 50% scale. Two of these specimens model a pre-1971 Caltrans prototype, and the two remaining specimens model the same prototype redesigned according to post-1994 Caltrans standards. A photograph of the rebar

assembly for one of these specimens is presented in Figure 1.2. The column longitudinal bars extend to the deck in the post-1994 design, but only halfway through the beam in the pre-1971 design. One of each design was tested pseudo-statically and one of each was tested dynamically. The loading protocol for each of the four tests contained a pulse and identical peak displacements in the same sequence. Only the loading rate varied from test to test.



**Fig. 1.2 Beam and column joint rebar assembly**

### **1.3 PULSE CHARACTERIZATION**

This report is concerned with the characterization of large velocity directivity pulses for the purpose of laboratory testing. The methods described yield a loading protocol that is both appropriate for the testing performed and representative of directivity pulses in general. It should be noted that these methods are not appropriate for the purpose of site response, for which an investigation of site-specific geometric and geologic considerations is imperative. In an effort to better understand the behavior of directivity pulses in general, the effects of several geometric and seismic considerations were investigated and the results will also be covered in this report; however, the application of these results to site response will not be discussed.

The need to define a single representative large velocity pulse for testing in the laboratory is readily apparent. A prerequisite to the definition of this pulse is an accurate characterization of large velocity pulses in general. A characterization of the pulse effect also includes a determination of what conditions give rise to a pulse and what factors affect the properties of the pulse. Also included in this report is a statistical analysis of the range of the property values for large velocity pulses. These statistical values are used specifically as tools in determining appropriate loading protocol for velocity pulse testing in the laboratory. The method used to determine the loading protocol for the PEER bridge pier project will be given as an example.

## 2 Background

There are many factors that affect the types of motions recorded at a site: the magnitude of the earthquake, the distance from the earthquake, topographic features, and the underlying soil stratigraphy are often the first factors to be considered. When a site lies within the near-fault region (less than 10 km), a unique set of factors controls the motion that is recorded. When these factors meet specific requirements the record is said to demonstrate directivity effects. This chapter will present current knowledge of directivity effects, their impact on engineered structures, and the availability of near-fault records.

### 2.1 DIRECTIVITY EFFECTS

One of the primary factors affecting motion in the near-fault region is the direction in which rupture progresses from the hypocenter along the zone of rupture. It is this factor which gives the directivity effect its name. “Directivity” refers to the direction of rupture propagation (see Fig. 2.1) as opposed to the direction of ground displacement (Abrahamson, 1998).

A site may be classified after an earthquake as demonstrating forward, reverse, or neutral directivity effects. If the rupture propagates toward the site and the angle between the fault and the direction from the hypocenter to the site is reasonably small, the site is likely to demonstrate forward directivity (Hall and Aagaard, 1998; Hall et al., 1995; Mahin and Hachem, 1998; and Somerville, 1997). If rupture propagates away from the site, it will likely demonstrate reverse directivity (Abrahamson, 1998). If the site is more or less perpendicular to the fault from the hypocenter it will likely demonstrate neutral directivity (see Fig. 2.2). The phrase “directivity effects” usually refers to “forward directivity effects”, as this case results in ground motions that are more critical to engineered structures.

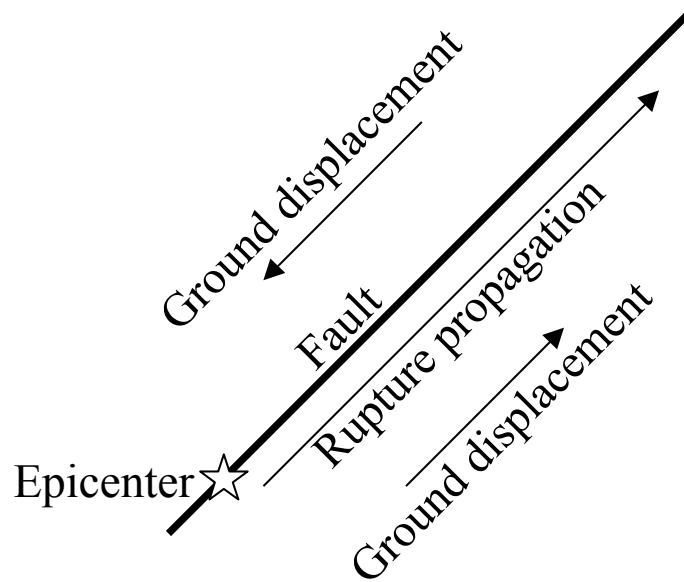


**Fig. 2.1 Directivity refers to the direction of rupture propagation**

Rupture often propagates at a velocity close to the velocity of shear wave radiation (Abrahamson, 1998; and Somerville, 1997). Because of this, energy is accumulated in front of the propagating rupture and is expressed in the forward directivity region as a large velocity pulse (Abrahamson, 1998; and Somerville and Graves, 1993). This is essentially the same principle as a sonic boom and may be thought of accordingly. It can be seen in Figure 2.3 that the seismic energy from each fault segment arrives at site A at almost the same time, resulting in a relatively short duration record containing large amplitudes. Site B, however, experiences the seismic energy distributed over a much larger period of time, resulting in a longer duration record with lower amplitudes.

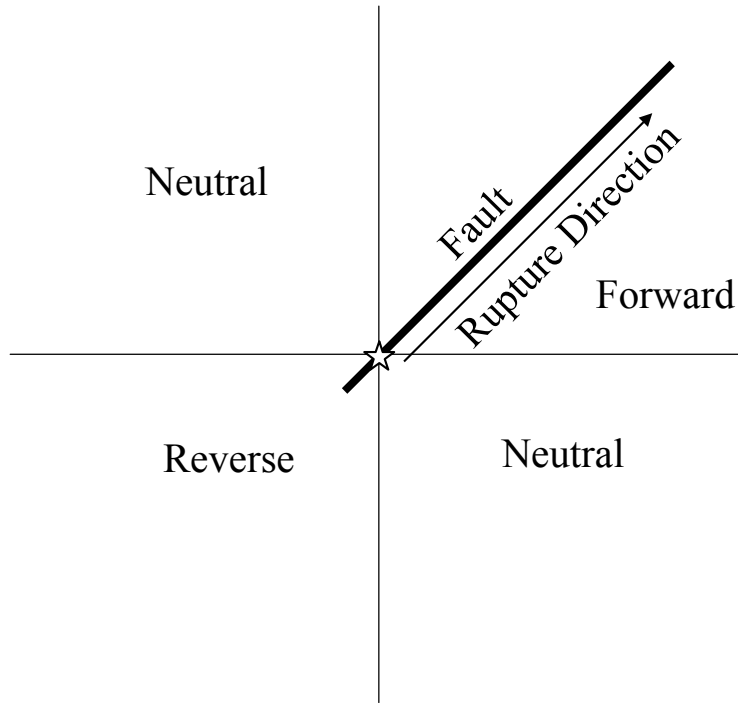


**Fig. 2.2 Defining a site as forward, reverse, or neutral directivity**

The SH (tangential motion) radiation pattern contains a maximum coincident with the direction of rupture propagation (see Fig. 2.4). By contrast, the SV (radial motion) radiation pattern demonstrates a minimum in the rupture direction. This results, counter-intuitively, in the large velocity pulse being visible only in the fault-normal direction, with no noticeable pulse in the fault-parallel direction (Abrahamson, 1998; and Somerville and Graves, 1993). In fact, the peak velocity in the fault-normal direction under these conditions is often twice the value of that in the fault parallel direction (Mayes and Shaw, 1997). For sites within 10 km of the rupture surface, one would expect to see a pulse in the same direction as the ground slippage, that is, in the fault-parallel direction. Indeed, if it is not filtered out of the record, a static residual displacement is visible; however, this static displacement does not correspond to a pulse in the velocity time history.

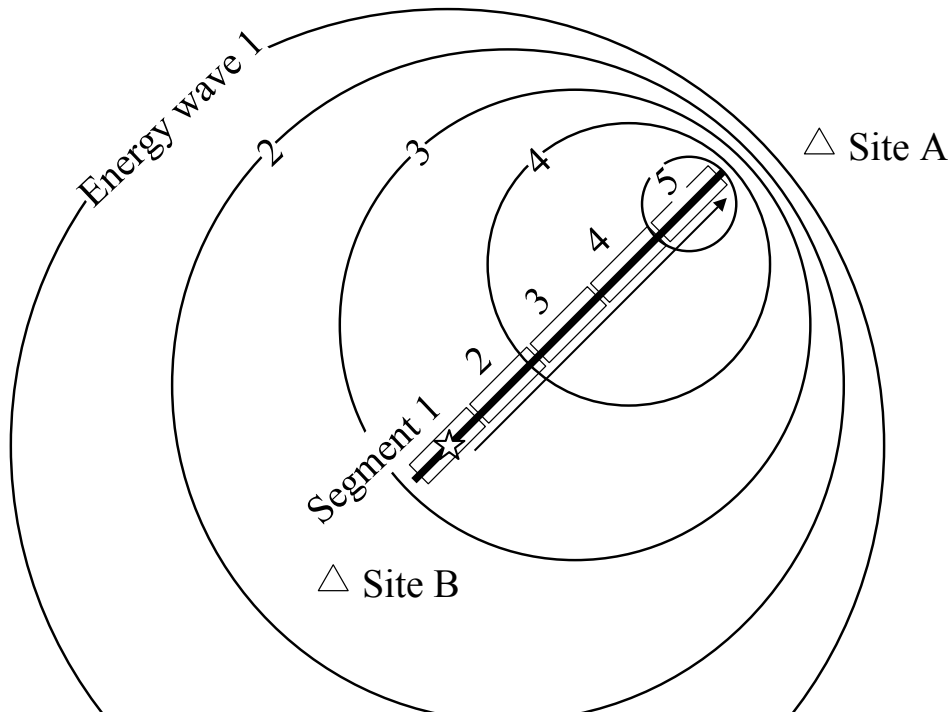


**Fig. 2.3 Effect of accumulation of seismic energy (after Abrahamson, 1998)**

These velocity pulses vary greatly in shape, peak magnitude, duration, and number of cycles. The dividing line between what is and what is not a large velocity directivity pulse is often subject to interpretation, however it is essential to this study to set clear parameters in defining which pulses to include.

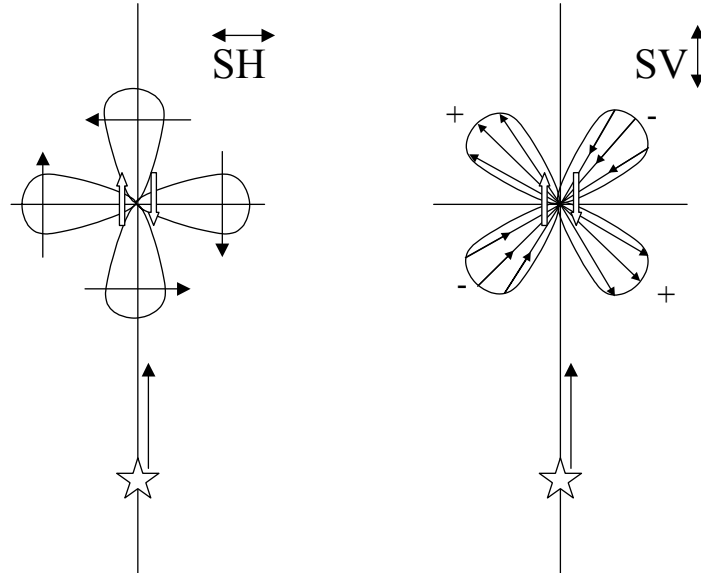


**Fig. 2.4 The large velocity pulse occurs in the fault-normal direction (after Somerville, 1993)**

## **2.2 IMPLICATIONS FOR ENGINEERED STRUCTURES**

There is little doubt about the significance of near-fault effects for engineered structures. Each new earthquake reveals inadequacies in the current standard of practice. Awareness of the importance of near-fault effects dates back as far as the 1971 San Fernando earthquake; however, significant code reform did not occur until after the Northridge earthquake of 1994.

The Sylmar Olive View Medical Center (Fig. 2.5) suffered extensive damage during the San Fernando earthquake in 1971. In-depth analysis of the damage to the building indicates that several design flaws and construction errors are responsible for the majority of the failures. However, the overall damage pattern and the large residual displacements visible in the complex are attributed to the near-fault large velocity pulse experienced at the site during the earthquake (Bertero et al., 1978).



**Fig. 2.5 Sylmar Olive View Medical Center**

Much of the current drive for research in near-fault effects stems from information gathered during and after the 1994 Northridge earthquake (Hall et al., 1995). A catalog of permanently displaced buildings in the near-fault region reveals some surprising evidence of the impact of large velocity pulses on engineered structures (Attalla et al., 1998). A total of 66 buildings with residual displacements were cataloged, of which 92% (61) were displaced to the north or the south. None of the 61 buildings reported any component of displacement in the east or west direction. This would indicate an earthquake in which the shaking was much greater along one axis as compared to the other. This is exactly the situation present in many of the near-fault records. Further examination of buildings with residual drift reveals that of 59 buildings cataloged on the hanging wall, 92% (54) were displaced to the north only, with no component of lean in the southern direction. This is best explained by considering a single large pulse delivering the majority of the energy during the earthquake rather than more randomly distributed noise.

In contrast to data gathered on the response of buildings, information on the response of bridge columns to near-fault motion is lacking and much research needs to be done. Analyses of

Caltrans bridge design indicate possible inadequacies in accounting for near-fault effects (Mahin and Hachem, 1998; Mayes and Shaw, 1997).

Mayes and Shaw (1997) performed an analytical study of the response of 16 Caltrans bridge columns to 20 time histories. Seven of these were originally recorded motions frequency scaled to comply with Caltrans Bridge Design Specifications (BDS) 0.6g design spectra with a soil profile Type C (marginal soil) corresponding to a magnitude 7.25 event (ATC, 1996). Ten of the records were generated records and three were unaltered, recorded near-fault motions. The results of these simplified analytical models indicate that the majority of the columns studied were inadequately designed to respond to a near-fault large velocity pulse. The elastic displacement obtained from the design spectra is a poor indicator of the inelastic displacement due to near-fault motion. To account for the majority of the displacements resulting from near-fault records, the elastic spectral displacement must be multiplied by two. Mayes and Shaw also indicate that the elastic displacements from the actual near-fault records are not a good predictor of the nonlinear displacements.

Mahin and Hachem (1998) indicate the possibility of using elastic methods as the basis of design in most cases. However, it appears that when the elastic period of the structure is shorter than the duration of any probable damaging pulse, elastic methods may not yield a conservative design.

### **2.3 AVAILABILITY OF NEAR-FAULT RECORDS**

Perhaps the greatest limitation to the study of near-fault effects is the relatively limited amount of seismic recordings from the near-fault region. While seismographs and seismic recordings have been in place for many years, the development of strong motion seismographs is a relatively recent event. These instruments must be able to accurately record ground accelerations approaching or surpassing the acceleration of gravity. Cost has prohibited installment of large numbers of these instruments. Furthermore, the inability to predict the time, location, and rupture zone of a large earthquake on any given fault makes strategic placement of a single seismograph with the intent to capture a pulse extremely difficult. In addition, these instruments have been historically difficult to maintain, resulting in a significant number of stations recording no or unusable data after each event. As a result, until 1994 and 1995, almost all recorded

ground motions were of earthquakes too far away to exhibit a large velocity directivity pulse. Before this time, those few stations lucky enough to be in the right place at the right time to record a pulse were not capable of recording such excessive ground motions.

The recent earthquakes in Turkey (August 17, 1999, Kocaeli) and Taiwan (September 20, 1999, Chi-Chi) have significantly increased the amount of data available in the near-fault, forward directivity region. Unfortunately, these data came after a majority of this work was completed. The work completed prior to the availability of the data will be reported with respect for the historical chronology of events as they occurred. The effect of these new data sets on previous results and conclusions will be discussed in Chapter 6.

Based on the literature review, it is clear that significant gaps exist in the current knowledge of large velocity directivity pulses. A basic characterization of large velocity directivity pulses, development of testing protocol representing near-fault motion, laboratory testing of bridge components and systems designed according to the current Caltrans code, and performance assessments of bridge components and structures are all areas that require further study. This report will address characterization of large velocity directivity pulses and the development of the testing protocol representing the pulses.

## 3 Data Collection

The majority of the records analyzed in this project came from the PEER database assembled by Walt Silva (Silva, 1998). This database greatly aided the study by providing a large number of records with consistent processing. Use of this database also provides a measure of continuity between other PEER research projects. This database consists of 1084 records from 140 earthquakes. Analysis of the records contained in this database returned 30 records within 20 km of the fault rupture of a moment magnitude 6 or greater earthquake. These 30 records were augmented with 4 more from other sources to make a total of 34 records. This chapter will discuss analysis of these 34 records for a large velocity pulse, how the pulses were used in the study, methods of analysis, and statistical results of the pulses retrieved from the records.

### 3.1 DESCRIPTION OF RECORDS

In this phase of the study, 34 records were analyzed from 13 different earthquakes. Ten of these records contained no pulse, resulting in a total of 24 pulses extracted from the catalog. The study limited the catalogue to earthquakes of  $M_w \geq 6$  or larger and to records from stations lying closer than 20 km to the rupture surface. These records are listed in Table 3.1. The largest magnitude earthquake represented is the 1978 Tabas, Iran, earthquake with a  $M_w = 7.4$ . The smallest magnitude earthquake represented is the 1966 Parkfield earthquake with a moment magnitude of 6.1. The station closest to the fault rupture surface was at Kobe University, a distance of 0.2 km during the 1995 Kobe earthquake. The station farthest from the rupture surface was the Tarzana Nursery, at 15.6 km, during the 1994 Northridge earthquake. It should be noted, however, that this is an exceptional case and no other record from farther than 10 km was found to contain a pulse. In fact, the next farthest station location was the Sepulveda Veterans Hospital located 8.4 km from the rupture surface during the Northridge earthquake.

In agreement with previous studies, the pulse was found to act primarily in the fault-normal direction. The column labeled “Pulse Direction” in Table 3.1 indicates the compass heading in which the largest peak velocity is acting. If this direction corresponds to either the fault-normal or the fault-parallel direction, it is indicated by FN or FP respectively. If on the other hand, the principle direction of the pulse does not correspond to either the fault normal or the fault parallel, the direction is indicated as an azimuth angle in degrees. This property is best illustrated by plotting the particle velocity trace. As an example, the particle velocity trace for the Rinaldi Receiving Station record from the Northridge earthquake is shown in Figure 3.1. The velocity pulse is easily visible looping out in the fault-normal direction.

**Table 3.1 All records analyzed for the presence of a pulse**

Date	Quake	Moment Magnitude	Station	Distance (km)	Pulse Direction
06/28/66	Parkfield, USA	6.1	Parkfield Cholame 5W <sup>1</sup>	6.8	FN
06/28/66	Parkfield, USA	6.1	Parkfield Cholame 8 <sup>1</sup>	8.0	No Pulse
02/09/71	San Fernando, USA	6.6	Pacoima Dam <sup>1</sup>	1.7	FN
05/17/76	Gazli, USSR	7.4	Karakyr Point <sup>1</sup>	3.0	No Pulse
09/16/78	Tabas, Iran	7.4	Dayhook <sup>1</sup>	17.0	No Pulse
09/16/78	Tabas, Iran	7.4	Tabas <sup>1</sup>	1.2	FN
12/23/85	Nahanni, Canada	6.8	Site 1, Iverson <sup>1</sup>	6.0	FN
12/23/85	Nahanni, Canada	6.8	Site 2, Slide Mountain <sup>1</sup>	8.0	FP
12/23/85	Nahanni, Canada	6.8	Site 3 <sup>1</sup>	16.0	No Pulse
07/08/86	North Palm Springs, USA	6.2	North Palm Springs Post Office <sup>1</sup>	4.0	FN
11/24/87	Superstition, USA	6.6	Superstition Mountain <sup>1</sup>	4.3	No Pulse
11/24/87	Superstition, USA	6.6	Westmoreland Fire Station <sup>1</sup>	13.3	No Pulse
10/18/89	Loma Prieta, USA	7.0	Capitola <sup>1</sup>	14.5	No Pulse
10/18/89	Loma Prieta, USA	7.0	Corralitos <sup>1</sup>	3.4	No Pulse
10/18/89	Loma Prieta, USA	7.0	Lexington Dam <sup>2</sup>	5.3	FN
10/18/89	Loma Prieta, USA	7.0	Los Gatos Presentation Center <sup>1</sup>	5.9	FN
03/13/92	Erzincan, Turkey	6.9	Erzican <sup>1</sup>	5.2	FN
04/25/92	Cape Mendocino, USA	7.0	Cape Mendocino Petrolia <sup>3</sup>	8.5	FN
04/25/92	Cape Mendocino, USA	7.0	Petrolia General Store <sup>3</sup>	9.5	324
06/28/92	Landers, USA	7.3	Joshua Tree <sup>1</sup>	10.6	No Pulse
06/28/92	Landers, USA	7.3	Lucerne Valley <sup>1</sup>	2.1	FN
01/17/94	Northridge, USA	6.7	Arleta Nordhoff Ave. fire station <sup>1</sup>	8.3	263
01/17/94	Northridge, USA	6.7	Jensen Filtration Plant <sup>1</sup>	5.4	FN
01/17/94	Northridge, USA	6.7	Newhall Fire Station <sup>1</sup>	6.2	FN
01/17/94	Northridge, USA	6.7	Rinaldi Receiving Station <sup>1</sup>	6.5	FN
01/17/94	Northridge, USA	6.7	Saticoy <sup>1</sup>	12.8	No Pulse
01/17/94	Northridge, USA	6.7	Sepulveda VA Hospital Bldg 40 <sup>1</sup>	8.4	81
01/17/94	Northridge, USA	6.7	Sylmar Converter Station <sup>1</sup>	5.2	FN
01/17/94	Northridge, USA	6.7	Sylmar Converter Station East <sup>1</sup>	5.3	FN
01/17/94	Northridge, USA	6.7	Sylmar Olive View Medical Center <sup>1</sup>	5.3	FN
01/17/94	Northridge, USA	6.7	Tarzana Cedar Hill Nursery <sup>1</sup>	15.6	87
01/16/95	Kobe, Japan	6.9	Kobe (JMA) <sup>1</sup>	0.6	12
01/16/95	Kobe, Japan	6.9	Kobe University <sup>1</sup>	0.2	FP
01/16/95	Kobe, Japan	6.9	Takatori <sup>4</sup>	0.3	FN

Record sources: 1. Silva, 1998; 2. Parsi, 1998; 3. ICS, 1999; 4. Somerville, 1998.

Distance is the closest distance to fault rupture.

Pulse direction: FN = Fault Normal, FP = Fault Parallel. Numerical values indicate degrees counterclockwise from north

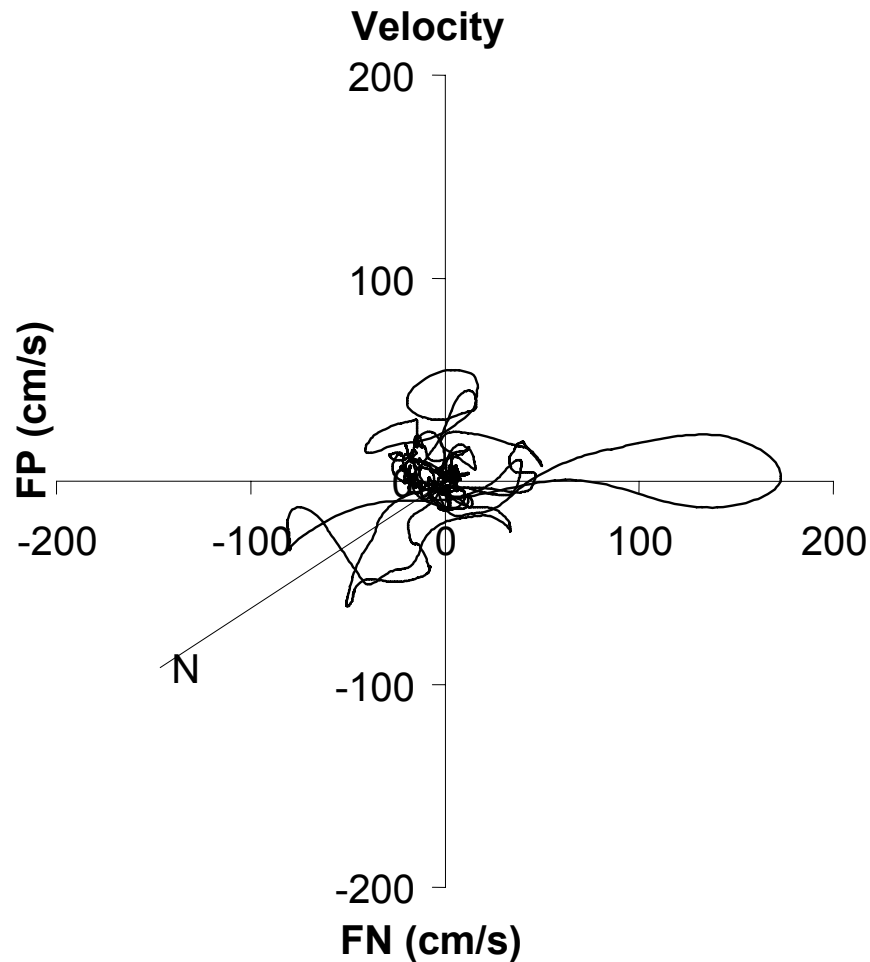


**Fig. 3.1 Velocity particle trace from the Rinaldi Receiving Station, Northridge earthquake**

One record from the 1971 San Fernando earthquake was also found to contain a directivity pulse. No other recording stations were located close enough to the rupture surface to capture a directivity pulse. This earthquake, which occurred on February 9, 1971, was a thrust fault earthquake that resulted in a pronounced directivity pulse experienced by the Pacoima Dam. The recording station that captured this pulse was located on the left abutment over highly jointed diorite gneiss.

On September 16, 1978, a magnitude 7.4 earthquake shook Tabas, Iran. The pulse recorded during this earthquake is one of the distinctive pulses in the database, with a duration of 4.5 seconds. Unique to this pulse is the location of the pulse within the record. The typical pulse occurs at the beginning of the record. This pulse, however, occurs toward the middle.

The Nahanni, Canada, earthquake of December 23, 1985 occurred in the Nahanni region of the Mackenzie Mountains in the Northwest Territories. Before the 1985 series of earthquakes, this region was thought to be relatively quiet seismologically. The Nahanni earthquake produced not only a primary pulse but also a secondary pulse later in the record. Two recording stations (Iverson, and Slide Mountain) captured these pulses.

The 1986 North Palm Springs earthquake caused over \$4 million in damage. 29 people were injured and 51 homes were damaged or destroyed. A station at the North Palm Springs post office recorded a very pronounced directivity pulse during the earthquake. This pulse contains a peak velocity of 74 cm/s.

The 1989 Loma Prieta earthquake occurred at perhaps the worst possible time, during the evening rush hour when the traffic flow was just reaching its peak. The third game of the World Series had filled Candlestick Park. During the earthquake, pulses were captured at two locations, the Lexington Dam and the Los Gatos Presentation Center.

The Erzincan, Turkey, earthquake on March 13, 1992, gave another example of a near-fault record dominated by a directivity pulse. This strike-slip earthquake ruptured a 30 km segment of the North Anatolian fault in the Erzincan basin. It resulted in considerable damage to Erzincan and surrounding villages.

Two records with pulses were retrieved from the April 25, 1992, Cape Mendocino earthquake. The Cape Mendocino record contains the stronger of the two with peak velocities over 100 cm/s. This earthquake, together with its aftershocks, resulted in approximately \$60 million in damages.

The Lucerne Valley record from the June 28, 1992, Landers earthquake also contains a strong pulse with the longest duration of any in the database. This record is often used in comparison with the Joshua Tree record from the same earthquake to demonstrate the differences between forward and reverse directivity. The Lucerne record lies in the forward directivity region and demonstrates a significant pulse. The Joshua Tree station, on the other hand, lies in the reverse directivity region and demonstrates no pulse.

The January 17, 1994, Northridge earthquake gave the largest single contribution to the database, in terms of number of records with pulses. Nine records in total were found to contain pulses from this earthquake. The Northridge earthquake is also important from a historical standpoint as the first major earthquake to occur in an urban setting within near-fault range of many strong motion accelerometers. Because of its location and timing, it generated a large

amount of strong motion data. The knowledge gained from this earthquake alone was the impetus for significant discussion and even code reform.

The day before the first anniversary of the Northridge earthquake, a magnitude 6.9 earthquake shook Kobe, Japan. Data received from this earthquake served to confirm many principles derived from the Northridge earthquake. For this study, three pulses were extracted from the data collected during the Kobe earthquake: Kobe JMA, Kobe University, and Takatori.

### **3.2 PULSE RECOGNITION**

Data collection required a simple procedure for determining which records contain a pulse and which do not. The available literature on large velocity directivity pulses does not contain a quantitative definition of a large velocity pulse. Qualitative methods used to date can be summarized by two general requirements. The first is that the site must fill the geometric and seismologic requirements of forward directivity (discussed in Section 1.1). The second is that visual inspection of the velocity time history reveals a pulse-like shape. This section will describe in detail the quantitative definition used for this study to segregate those records containing a large velocity directivity pulse. It was determined from inspection of the records in Table 3.1 that those records containing a directivity pulse exhibit a peak velocity twice the value of any peak velocity outside of the pulse. Although other criteria were considered, this method was chosen for its simplicity and ease of calculation.

One other method of distinguishing directivity pulses deserves some discussion. This method involves taking the square of the velocities at each time step throughout the record. The pulse will then show up as a single or several large spikes. This method has the advantage of reporting only the absolute values of the velocity, automatically. Another advantage is the exaggeration of relatively high velocity pulses. Disparities between the pulse and the rest of the record are more pronounced and more easily distinguished visually. An example of the velocity squared time history is plotted in Figure 3.2 for the Northridge, Rinaldi Receiving Station record. The velocity time history is plotted above the velocity squared time history. The limiting criterion would then be that the peak velocity squared value must be four times the value of any other velocity squared value without the pulse. Note that this is identical to saying that the peak absolute velocity is twice the absolute velocity without the pulse.

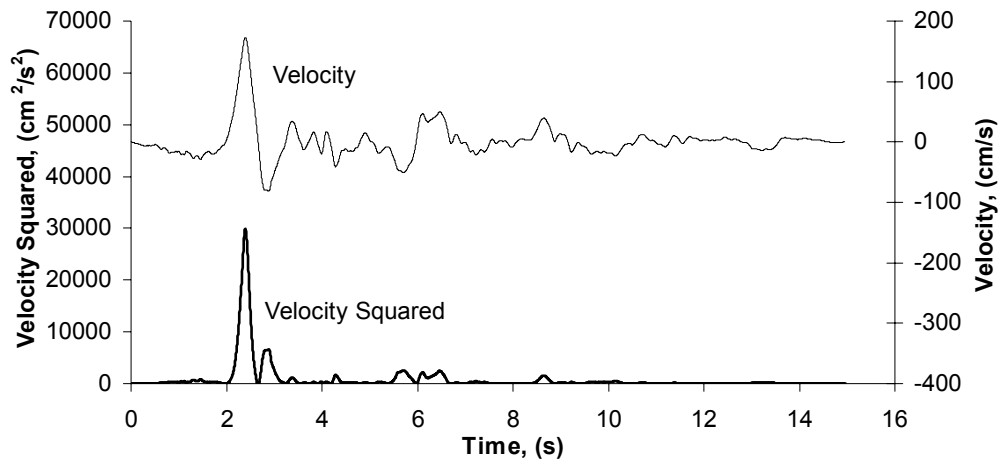


**Fig. 3.2 Velocity squared time history for the Rinaldi Receiving Station, Northridge earthquake**

### 3.3 ROTATION TO FAULT NORMAL

For each record analyzed, the data were first rotated to the fault-normal direction. This rotation was performed by a simple vector rotation (Somerville, 1997). If, as is often the case, the accelerometers are oriented with one measuring north-south (N) and the other measuring east-west (E), and the fault-normal direction is at an angle,  $\phi$  (measured clockwise from north), then the record can be rotated to the fault-normal direction (SN) by:

$$SN = N \cdot \cos(\phi) + E \cdot \sin(\phi)$$

This rotation is illustrated in Figure 3.3.

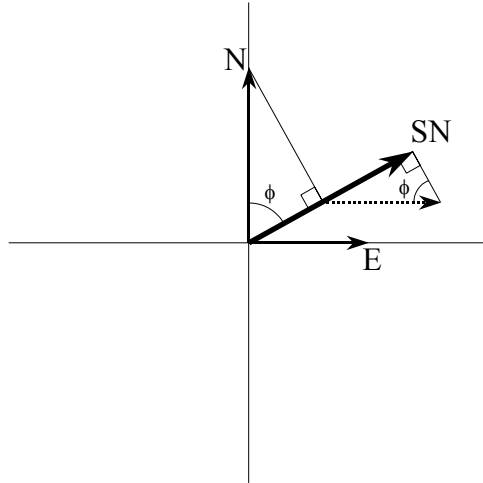


**Fig. 3.3 Acceleration in the fault-normal direction when the accelerometers are oriented north and east**

If the accelerometers are not oriented north-south and east-west, rotation becomes slightly more complex. For example, if accelerometer A measures the acceleration at an angle,  $\alpha$ , and accelerometer B measures the acceleration at an angle,  $\beta$ , where  $\alpha$  and  $\beta$  are orthogonal, then the acceleration in the fault-normal direction can be obtained by:

$$SN = A \cdot \cos(\phi - \alpha) + B \cdot \cos(\phi - \beta)$$

This case is illustrated in Figure 3.4.

One record in the database, the Lucerne record from the 1992 Landers earthquake, recorded motion on accelerometers that were not installed orthogonal to one another. Rotation of this record first required solving at each time step for the absolute acceleration vector that gave rise to the accelerations recorded on the two accelerometers. The absolute acceleration vector can be found by the intersection of the perpendiculars to the recorded accelerations (see Fig. 3.5).

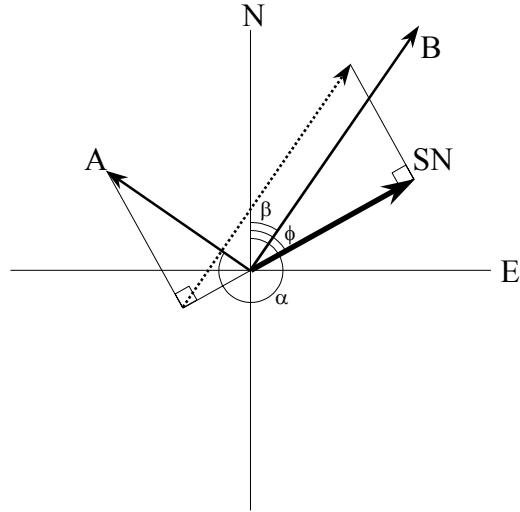


**Fig. 3.4 Acceleration in the fault-normal direction when the accelerometers are orthogonal**

The perpendiculars to the recorded accelerations are found by:

$$C_x = C_y \cdot \tan\left(\alpha + \frac{\pi}{2}\right) + A \cdot \sin(\alpha) - A \cdot \cos(\alpha) \cdot \tan\left(\alpha + \frac{\pi}{2}\right)$$

$$C_x = C_y \cdot \tan\left(\beta + \frac{\pi}{2}\right) + B \cdot \sin(\beta) - B \cdot \cos(\beta) \cdot \tan\left(\beta + \frac{\pi}{2}\right)$$

Solving this system of equations for  $C_y$  and  $C_x$  results in the absolute acceleration vector in Cartesian coordinates. The acceleration (SN is of interest in this discussion) in any direction ( $\phi$ ) can then be found by:

$$SN = C_y \cdot \cos(\phi) + C_x \cdot \sin(\phi)$$

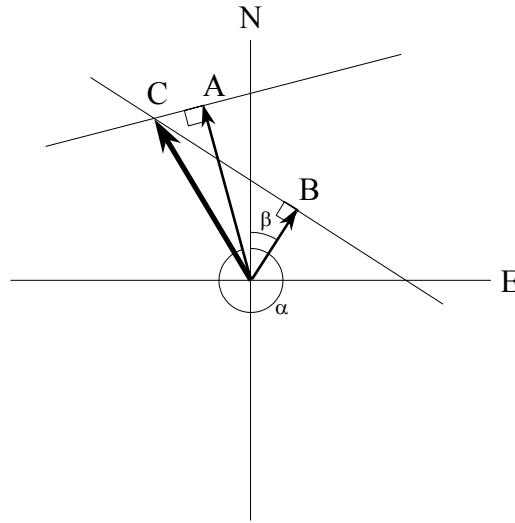


**Fig. 3.5 Recorded accelerations A and B result from the absolute acceleration vector, C**

### 3.4 TYPICAL PULSE

The intent of this study is to determine a single representative large velocity pulse to be used in laboratory testing. To this end, the pulses were analyzed to determine mean values that could be used in constructing a representative pulse. The average number of cycles of all pulses gathered was 1, although pulses were found ranging from 0.5 to 2 cycles. On average, the largest peak velocity value occurred during the first half cycle of the pulse. A list of the peak velocity values and the average period for each pulse as well as the record in which it was found is given in Table 3.2 below.

The maximum peak velocity value was 174 cm/s, found in the Takatori record from the Kobe earthquake. The minimum peak velocity value was 23 cm/s, found in the Cholame 5W record from the Parkfield earthquake. The average peak velocity value was 94 cm/s with a standard deviation of 44 cm/s.

**Table 3.2 Records containing pulses**

Date	Quake	Moment Magnitude	Station	Peak Vel (cm/s)	Period (s)
06/28/66	Parkfield, USA	6.1	Parkfield Cholame 5W <sup>1</sup>	23	0.5
02/09/71	San Fernando, USA	6.6	Pacoima Dam <sup>1</sup>	114	1.3
09/16/78	Tabas, Iran	7.4	Tabas <sup>1</sup>	121	4.5
12/23/85	Nahanni, Canada	6.8	Site 1, Iverson <sup>1</sup>	40	2.3
12/23/85	Nahanni, Canada	6.8	Site 2, Slide Mountain <sup>1</sup>	24	0.6
07/08/86	North Palm Springs, USA	6.2	North Palm Springs Post Office <sup>1</sup>	74	1.3
10/18/89	Loma Prieta, USA	7.0	Lexington Dam <sup>2</sup>	119	1.2
10/18/89	Loma Prieta, USA	7.0	Los Gatos Presentation Center <sup>1</sup>	93	2.6
03/13/92	Erzincan, Turkey	6.9	Erzican <sup>1</sup>	95	2.7
04/25/92	Cape Mendocino, USA	7.0	Cape Mendocino Petrolia <sup>3</sup>	125	3.7
04/25/92	Cape Mendocino, USA	7.0	Petrolia General Store <sup>3</sup>	63	1.2
06/28/92	Landers, USA	7.3	Lucerne Valley <sup>1</sup>	144	9.3
01/17/94	Northridge, USA	6.7	Arleta Nordhoff Ave. fire station <sup>1</sup>	26	1.0
01/17/94	Northridge, USA	6.7	Jensen Filtration Plant <sup>1</sup>	104	2.6
01/17/94	Northridge, USA	6.7	Newhall Fire Station <sup>1</sup>	121	1.1
01/17/94	Northridge, USA	6.7	Rinaldi Receiving Station <sup>1</sup>	173	1.3
01/17/94	Northridge, USA	6.7	Sepulveda VA Hospital Bldg 40 <sup>1</sup>	85	1.1
01/17/94	Northridge, USA	6.7	Sylmar Converter Station <sup>1</sup>	130	2.6
01/17/94	Northridge, USA	6.7	Sylmar Converter Station East <sup>1</sup>	116	2.6
01/17/94	Northridge, USA	6.7	Sylmar Olive View Medical Center <sup>1</sup>	123	2.3
01/17/94	Northridge, USA	6.7	Tarzana Cedar Hill Nursery <sup>1</sup>	65	1.9
01/16/95	Kobe, Japan	6.9	Kobe (JMA) <sup>1</sup>	74	1.3
01/16/95	Kobe, Japan	6.9	Kobe University <sup>1</sup>	34	1.7
01/16/95	Kobe, Japan	6.9	Takatori <sup>4</sup>	174	1.6
				<b>Peak Vel</b>	<b>Period</b>
				Maximum	174 9.3
				Minimum	23 0.5
				Mean	94 2.2
				Standard Deviation	44 1.8

Record sources: 1. Silva, 1998; 2. Parsi, 1998; 3. ICS, 1999; 4. Somerville, 1998.

The period of each pulse also gives a wide range of values. The maximum period was 9.3 sec found in the Lucerne record from the Landers earthquake. The minimum period was 0.5 sec found in the Cholame 5W record from the Parkfield earthquake. The average period was 2.2 sec with a standard deviation of 1.8 sec.

The typical large velocity directivity pulse can be described as a single cycle occurring at the beginning of the record. The peak velocity is around 100 cm/s and is found in the first half cycle. The duration of the pulse is approximately 2 s.

### 3.5 ATTENUATION RELATIONS

In order to gain a greater understanding of the factors affecting large velocity directivity pulses, a regression analysis was conducted. This analysis considered the effects of several geometric and seismological factors on the peak velocity and period of the directivity pulse. The factors analyzed in this study are the moment magnitude of the earthquake,  $M_w$ ; the distance to the rupture surface,  $r$ ; the directivity ratio,  $X$ ; and the directivity angle,  $\phi$ .

The directivity ratio,  $X$ , and the directivity angle,  $\phi$ , are measures of the directivity of the site in relation to the earthquake (Somerville, 1997). It should be noted that Somerville uses different symbols for the ratio and angle depending on whether the earthquake was a strike-slip or dip-slip earthquake. In this report, the symbols  $X$  and  $\phi$  will be used regardless of the type of earthquake. Somerville defines the ratio as the distance along the fault between the hypocenter and the site divided by the total length of the fault. For strike-slip, the ratio is measured horizontally, for dip-slip vertically. The angle is defined as the angle that the site and the hypocenter make with the fault. Again, this angle is measured horizontally for the strike-slip case and vertically for the dip-slip case.

A more general definition for the directivity ratio with respect to angle is used in this report to better accommodate the case of oblique faulting. In this definition,  $X$  is defined as the rupture surface area along the slip between the hypocenter and the station divided by the total rupture surface area. The  $\phi$  is defined as the angle that the station and the hypocenter make with the fault in the plane of slip perpendicular to the rupture surface. It should be noted that this definition is the same as Somerville's for pure strike-slip and pure dip-slip ruptures.

The correlation between these factors and the period and peak velocity is listed in Table 3.3. The geometric properties were unavailable for both records from the Cape Mendocino earthquake and the Tarzana record from the Northridge earthquake, and these records were therefore excluded from the correlation analysis. Except for those three records, all pulses listed in Table 3.2 were included in the analysis. These attenuation relations are developed again in Chapter 6 to reflect the additional information from the Kocaeli and Chi-Chi earthquakes.

**Table 3.3 Correlation values for period and peak velocity**

	Period	Log(Period)	Peak Vel	Log(Peak Vel)
$M_w$	0.6254	0.6621	0.3434	0.3567
$r$	-0.3550	-0.4290	-0.3044	-0.3263
$X$	-0.4514	-0.3272	0.0564	0.0659
$\phi$	-0.4060	-0.4245	-0.3649	-0.3939
$\text{Log}(M_w)$	0.6105	0.6554	0.3461	0.3602
$\text{Log}(r)$	-0.1529	-0.2110	-0.1423	-0.1243
$X \cos(\phi)$	-0.4229	-0.2921	0.0936	0.1052

These correlation values indicate that the log of the period of the pulse is weakly dependent on the moment magnitude and the distance to the rupture surface. The strongest correlation for the peak velocity is found between the log of the peak velocity and the directivity angle and the log of the moment magnitude.

Regression on the moment magnitude and the distance to the rupture surface to obtain the log of the period yielded an  $R^2$  value of 0.471. The coefficients resulting from this regression analysis are presented in equation form:

$$\text{Log}(\text{Period}) = -3.579 + 0.5770 \cdot M_w - 0.02153 \cdot r$$

The fit of this equation to the data is demonstrated in Figures 3.6 and 3.7.

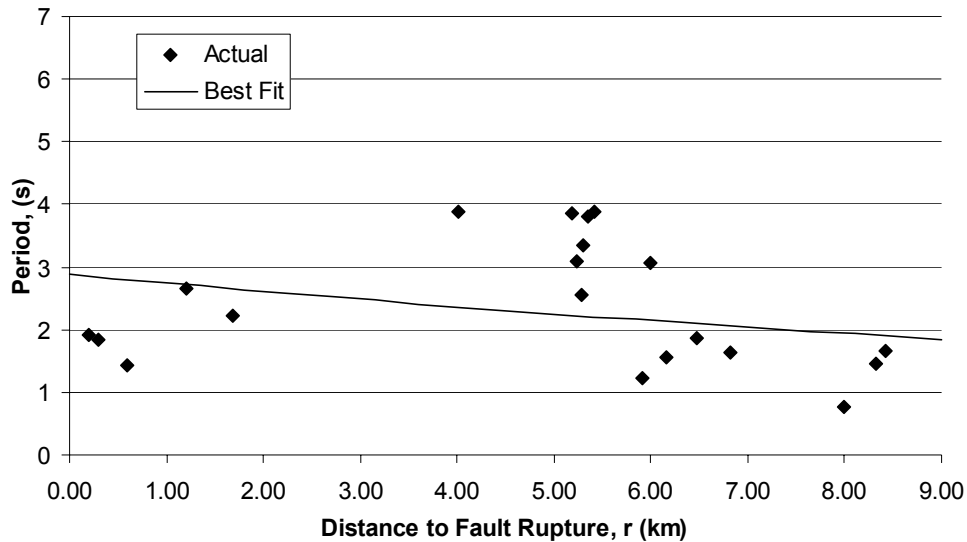


**Fig. 3.6 Period of the pulse predicted by  $r$ . Data are normalized to  $M_w = 7$ .**

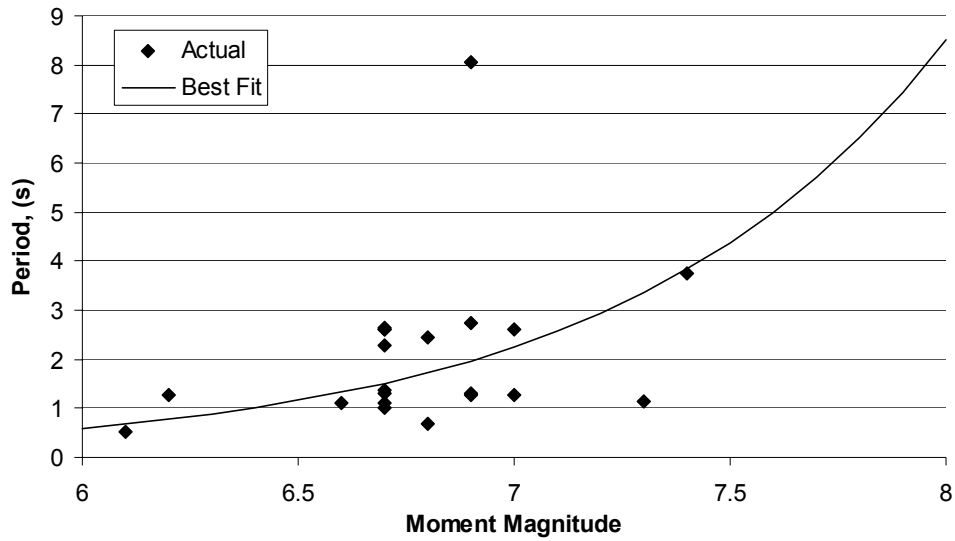


**Fig. 3.7** Period of the pulse predicted by  $M_w$ . Data are normalized to  $r = 5$  km.

Regression of the directivity angle and the log of the moment magnitude to obtain the log of the peak velocity resulted in a low  $R^2$  value of 0.1994. The residuals indicate two strong outliers. These outliers were removed and the analysis was performed again. The new results give a slightly improved  $R^2$  value of 0.4585. The coefficients from this analysis are given below:

$$\text{Log}(PV) = 6.444 - 0.01870 \cdot \phi - 5.022 \cdot \text{Log}(M_w)$$

The fit of this equation to the actual data is illustrated in Figures 3.8 and 3.9.

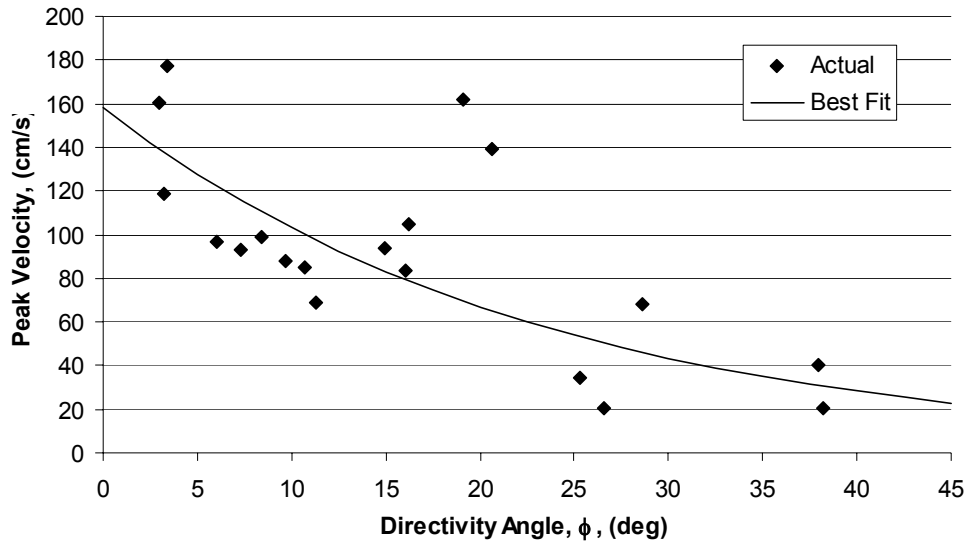


**Fig. 3.8** Peak velocity predicted by  $\phi$ . Data are normalized to  $M_w = 7$ .

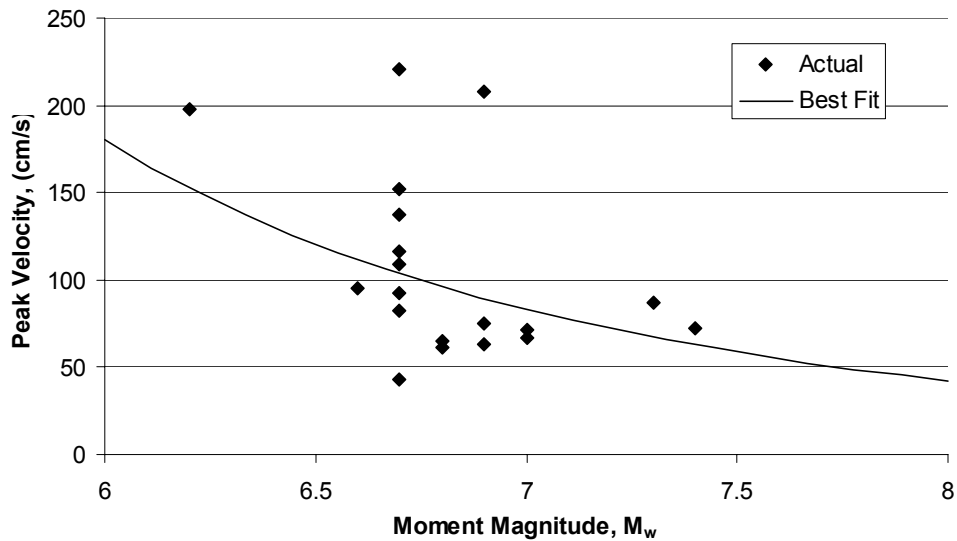


**Fig. 3.9** Peak velocity predicted by  $M_w$ . Data are normalized to  $\phi = 15^\circ$ .

The dependence of the period on the moment magnitude and the distance to the rupture surface was expected from current literature on directivity effects. The sign of the  $M_w$  coefficient in the peak velocity attenuation relationship was unexpected. It is generally

considered that the larger earthquakes will produce a larger peak velocity pulse. According to current theory, as  $\phi$  increases the pulse should lengthen in period and diminish in amplitude. This diminishing amplitude with increasing  $\phi$  is evident in this regression analysis.

## 4 Development of the Mean Pulse

One objective of this research was to obtain a single representative large velocity directivity pulse that could be used in laboratory testing. The laboratory testing at UCSD was designed to determine the response of bridge components, subassemblages and systems to such a pulse. This representative pulse must capture reasonable pulse characteristics of peak velocity, duration, number of cycles, and shape. It was also desired to represent a pulse that would be both realistic and structurally significant to the prototype. The development of the mean pulse as a basis for the various loading protocols will be discussed in this chapter.

### 4.1 EXTRACTION OF THE DIRECTIVITY PULSES

In order to obtain a single representative pulse, all pulses in the database needed to be extracted and normalized. A full cycle of each pulse was extracted from each time history containing a pulse, regardless of whether that specific pulse consisted of greater or fewer numbers of cycles. If the pulse contained more than one cycle, the pulse was extracted beginning at the half cycle containing the largest absolute peak velocity value. If the pulse was less than one cycle, an extra half cycle was extracted from the record after the pulse. All of these records are plotted in Figure 4.1. The records are listed in chronological order by the date of the earthquake. The pulse extracted is shown in bold on top of each record.

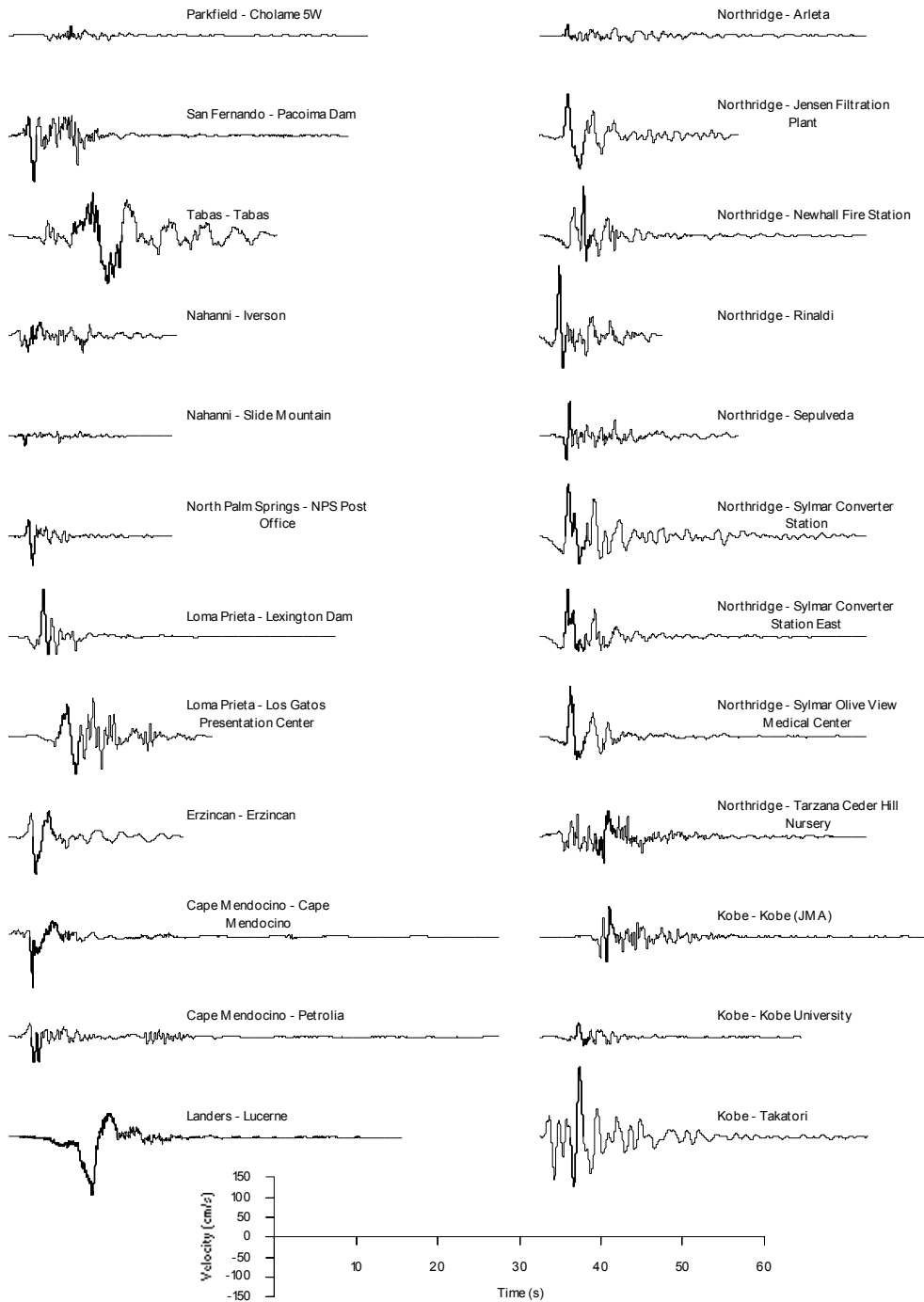


**Fig. 4.1 All records found to contain a pulse. The pulse is in bold.**

All the extracted pulses are plotted in Figure 4.2. The range of peak velocity values and duration of the pulse is readily apparent in this figure.

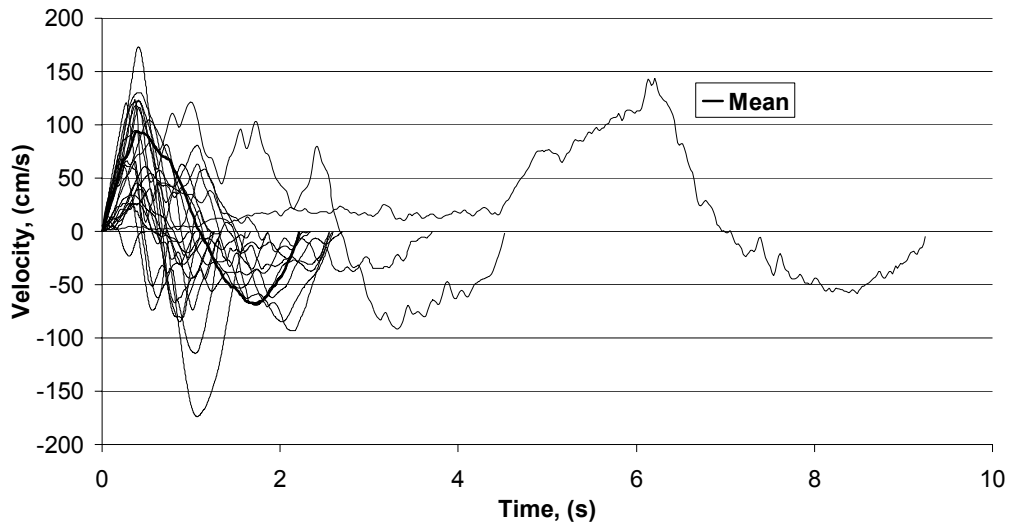


**Fig. 4.2 Comparison of all cataloged pulses and the mean pulse**

## 4.2 NORMALIZATION OF PULSE RECORDS

In order to obtain a mean representative pulse, each pulse needed to be normalized such that the properties of each pulse would average constructively. This section will discuss the procedure followed to normalize the velocity pulse time histories.

After extraction of the pulses, each pulse time history was modified by linear interpolation, to consist of the same number of data points. A time step was chosen such that each pulse matched the average period. Each pulse was analyzed for the sign of the first peak velocity. If the first peak velocity was negative, the pulse was inverted by multiplying each data point by negative one to make each pulse phase consistent. This was done to ensure that the values at each time step were averaged constructively. It should be noted that the process of inverting the record does not change the properties of the pulse and is equivalent to rotating the record 180°.

### 4.3 CONSTRUCTION OF THE MEAN PULSE

This section will present the method used to combine the normalized large velocity directivity pulses to form a single representative pulse. This mean pulse captures the average values of duration, amplitude, number of cycles, and shape. The mean pulse will be used to determine the loading protocol for laboratory testing.

At each time step the velocity values of all pulses were summed and the result was divided by the number of pulses to yield a new time history. Because the peak velocities do not occur at the same time in each record, the peak velocity value in this new time history was less than the average peak velocity from all records in the catalog. To compensate for this the new record was scaled to match the value of the average peak velocity, and the result is the mean pulse time history. This mean pulse is plotted in Figure 4.3.

The procedure produced a pulse for use in testing which captures the average properties of duration, period, peak velocity, and shape from a significant number of large velocity pulses. It should be noted here that the purpose of this pulse was for laboratory testing. The procedure followed is a relatively simplistic method and would not be sufficient for a seismic site response analysis. Accurate characterization of a directivity pulse for the purpose of hazard assessment at a specific site must include some consideration for geologic (e.g., local faults and soil stratigraphy) and geometric (e.g. distance to possible fault rupture) characteristics of the site. It is apparent from Table 3.2 and Figures 4.1 and 4.2 that a wide range of values is possible for the period and magnitude of a directivity pulse. For laboratory testing, it is desirable to find a pulse which will be meaningful to the purpose of the testing. For hazard assessment at a site however, the pulse should represent the range of values possible to be achieved at that location.

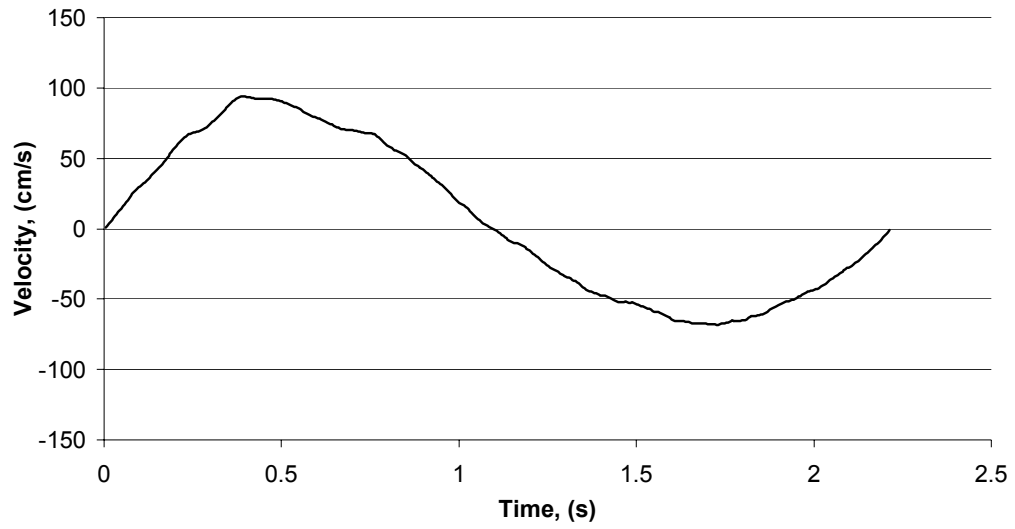


**Fig. 4.3 Mean large velocity pulse scaled to the average peak velocity value**

## **5 Characterization of the Loading Protocol**

The development of the various loading protocols will be described in this chapter. The factors affecting the loading protocol come from two primary sources: the structural prototype and laboratory testing set up. The structural prototype affects the loading protocol by dictating the most vulnerable period of the pulse. Also, since the tests were performed by applied displacements to the specimen rather than an inertial response on the shake table, the prototype structure was modeled analytically to determine the response of the structure to the input pulse motion. It was this response rather than the pulse that was used as the loading protocol in the laboratory tests.

The laboratory test set up affected the loading protocol primarily in the time domain. If the test was to be performed pseudo-statically, the peak displacements were reached with a constant velocity, with halts at the peaks and at other points of interest during the record. For the tests performed dynamically, the displacement time history was modified to sine and haversine forms in order to eliminate excessively high accelerations. The remainder of this chapter details the procedures followed in determining the loading protocols.

### **5.1 RESPONSE OF THE PROTOTYPE COLUMN**

The next step in defining the testing protocol is to determine the response of the prototype column to the mean near-fault large velocity pulse. The relative displacement between the top of the column and the ground was controlled directly and must, therefore, be defined by the response of the structure to the motion of the ground. Properties of the prototype column are given in Table 5.1.

**Table 5.1 Properties of the prototype column**

<b>Property</b>	<b>Value</b>
Height	16.46 m
Diameter	183 cm
Reinforcing	21 Bars, #18
Area of steel	542 cm <sup>2</sup>
Concrete strength	28 MPa
Steel strength	455 MPa

The response of the column was obtained from the program NONLIN (Charney, 1997). This program solves for the response of a nonlinear, single-degree-of-freedom structure. The nonlinear properties are modeled by a bilinear stiffness curve. The NONLIN program was chosen because of its simplicity. The simplicity of the input pulse displacement and the simplicity of the structural model do not warrant the use of a more complex program to obtain the prototype response. The values used to model the column in the NONLIN program are given in Table 5.2.

The forcing function is the mean near-fault large velocity pulse. Trailing zeros were added to the end of the mean pulse to force NONLIN to calculate several cycles of the free response of the structure after completion of the pulse. The output values from NONLIN are given in Table 5.3. The respective displacement and velocity time history response of the column is shown in Figure 5.1.

**Table 5.2 Properties of the single-degree-of-freedom model**

<b>Property</b>	<b>Value</b>
Initial stiffness	230 kN/cm
Strain-hardening stiffness	9 kN/cm
Structure yield strength	1100 kN
Yield displacement	5 cm
Weight	7250 kN
Damping	2 % Critical
Mass	739000 kg
Circular frequency	5.6 radians/s
Cyclic frequency	0.89 Hertz
Period of vibration	1.1 s
Damping constant	1.7 kN-s/cm

**Table 5.3 Response of the single-degree-of-freedom column**

<b>Measurement</b>	<b>Value</b>
Maximum inertial force, I	2870 kN
Maximum damping force, D	131 kN
Maximum spring force, S	1390 kN
Maximum damping + spring force	1410 kN
Maximum total force (D+S+I)	2880 kN
Maximum computed displacement	37 cm
Maximum computed velocity	79 cm/s
Maximum computed acceleration	389 cm/s <sup>2</sup>
Number of yield excursions	3
Displacement ductility demand	7.8

The next step in preparing the displacement time history for use as the testing protocol is to simplify the response of the column. First, the free-vibration response at the end of the record was removed. Then the response of the prototype column was simplified to a saw-toothed displacement time history and a box-shaped velocity time history. These values are given in Table 5.4 below. The displacement and velocity time histories are plotted in Figure 5.2.

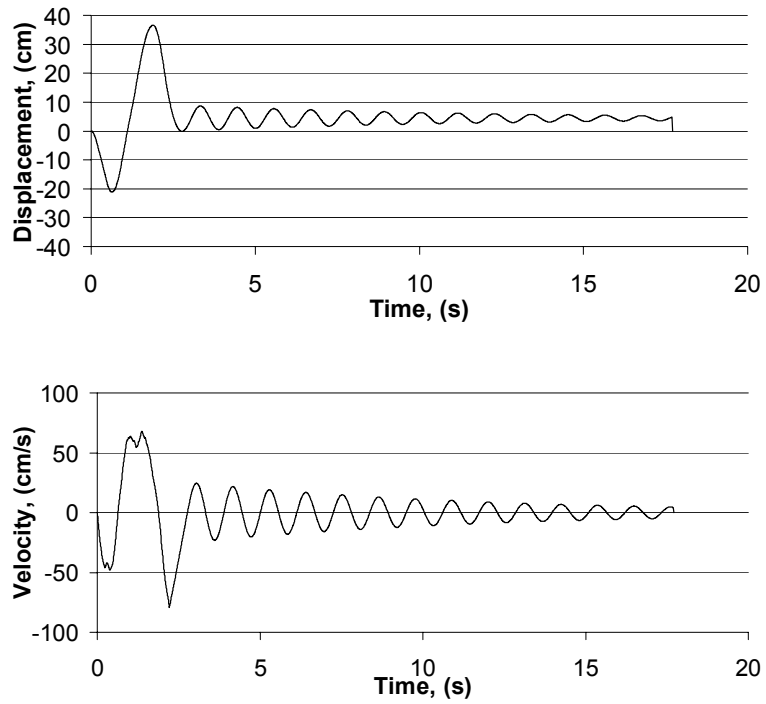


**Fig. 5.1 Analytical response of the column to the mean large velocity pulse**

**Table 5.4 Simplified column response values**

<b>Time (s)</b>	<b>Disp (cm)</b>	<b>Vel (cm/s)</b>
0.000	0.000	-33.402
0.633	-21.147	46.271
1.882	36.623	-43.309
2.727	0.000	

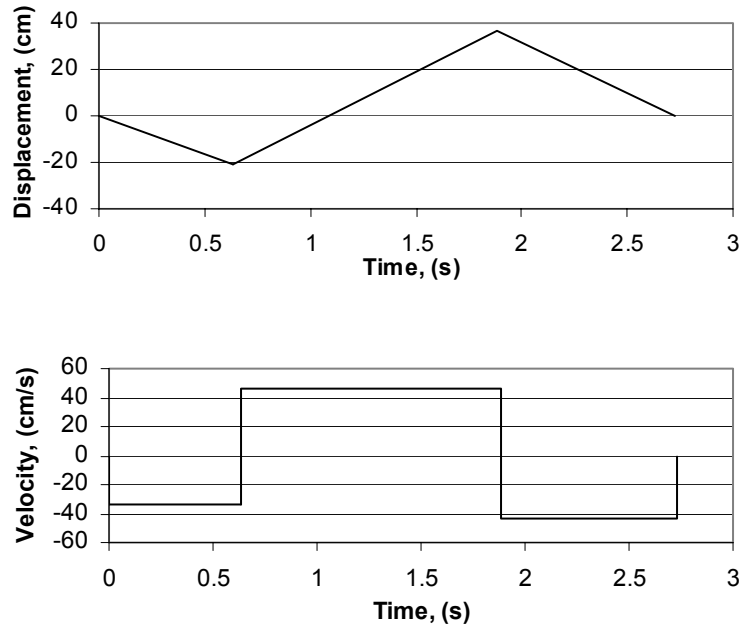


**Fig. 5.2 Simplified analytical column response time history**

These time histories must also be scaled to match the scaling factor of the columns to be tested. The columns were designed to 22% scale of the prototype column. The values in the time histories were divided by 4.5 to match this scaling factor. The resultant values are listed in Table 5.5. These simplified and scaled time histories (displacement and velocity) are plotted in Figures 5.2 and 5.3.

**Table 5.5 Simplified column response values scaled by 22%**

Time (s)	Disp (cm)	Vel (cm/s)
0.000	0.000	-7.423
0.633	-4.699	10.283
1.882	8.138	-9.624
2.727	0.000	

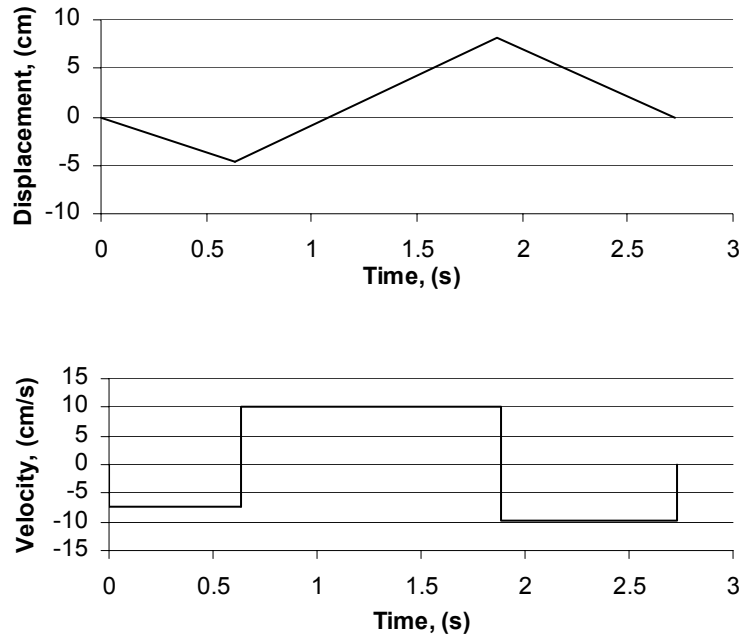


**Fig. 5.3 Simplified analytical column response scaled by 22%**

One goal of the loading protocol was to match displacements with testing done at other universities. This was done in order to facilitate comparison between various specimens. UCI, the first university to test, provided UCSD with the exact displacement time history followed during their test. The testing at UCSD attempted to replicate this loading as closely as possible.

The loading sequence after the pulse subjects the column to progressively larger levels of drift. It gives three excursions in each direction into each of the following percent drifts (in order): 0.5, 1.0, 1.5, 2.0, 3.0, 4.0, 5.0, and 6.0. These cycles following the pulse are not intended to simulate the remainder of an earthquake, but rather to determine the effect of the pulse on the residual strength of the specimen. An identical specimen was tested previously under the same cyclic scenario but without the pulse. Comparison of the performance of the two specimens with identical loading, except for the pulse at the beginning of one, will allow insights into the effect of the pulse on the residual strength of the column. This displacement time history is plotted in Figure 5.4.

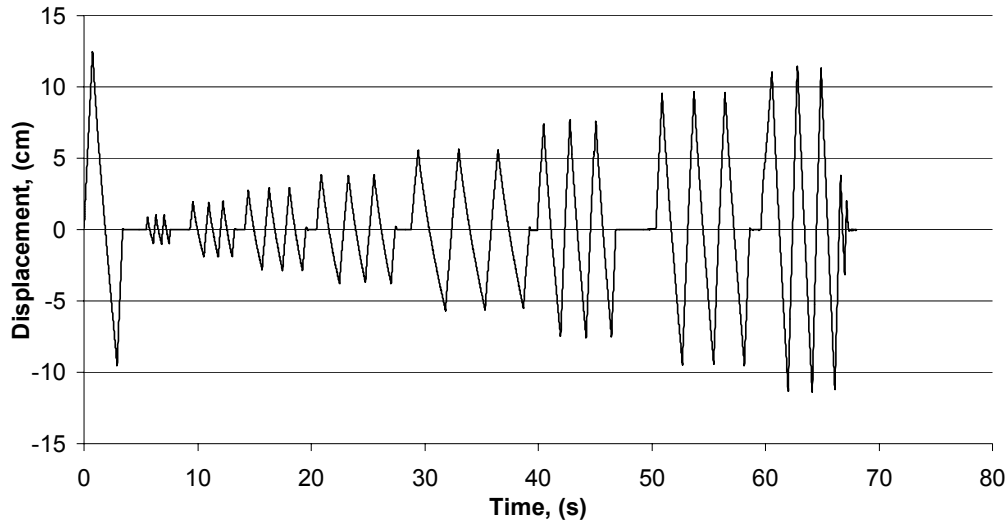


**Fig. 5.4 Displacement time history for the first test**

This test was performed dynamically with an actuator. The second test follows the same displacement trace as test one but under a pseudo-static regime, stopping at the displacement peaks and at other points of interest during the test.

The third test was performed on the shake table; however, the top of the column was pinned, the displacements were prescribed and the column was not allowed to respond under inertial loading. This permitted a more accurate reproduction of the displacement time histories from the other tests conducted at UCSD and UCI. The shake table was able to deliver much higher velocities than are possible with the other actuators available in the lab. In addition to the higher velocities, there were several other minor differences between the displacement time histories for the first and third test. The saw-toothed time history was smoothed out to a sinusoidal time history to avoid overly high accelerations. Several seconds of zeros were added at the beginning, the end, after the pulse, and in-between each successive series of drift level excursions. This displacement time history is plotted in Figure 5.5 below. Details of the column testing can be found in Orozco (2001).

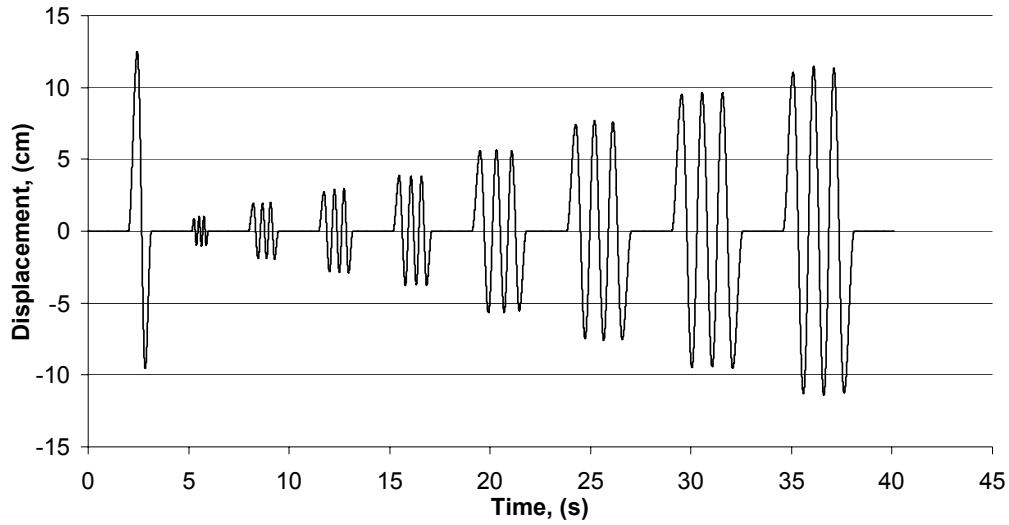


**Fig. 5.5 Displacement time history for the third test**

## 5.2 RESPONSE OF THE PROTOTYPE JOINT

The four joint specimens were based on different prototypes and therefore the response for this prototype required a separate analysis. The properties of the prototype column are listed in Table 5.6.

**Table 5.6 Column prototype properties for the joint specimens**

<b>Property</b>	<b>Value</b>
Height above ground	7.32 m
Diameter	122 cm
Reinforcing	16 Bars, #18
Area of steel	413 cm <sup>2</sup>
Concrete strength	28 MPa
Steel strength	276 MPa

The prototype structure for the beam-column joint specimens was built on continuous column pile connections with no pile cap. The effect of this added flexibility was modeled by

considering an equivalent depth to fixity of 1 pile diameter, or 1.22 m. The property values for the pile are given in Table 5.7.

**Table 5.7 Pile prototype properties for the joint specimens**

<b>Property</b>	<b>Value</b>
Depth below ground	1.22 m
Diameter	122 cm
Reinforcing	12 Bars, #18
Area of steel	310 cm <sup>2</sup>
Concrete strength	28 MPa
Steel strength	276 MPa

The computer program “Ruaumoko” (Carr, 1998) was used to determine the response of the prototype structure for the joint specimens. Ruaumoko is an inelastic dynamic analysis program with a robust library of elements and hysteretic rules for modeling two-dimensional frame structures. The program was set to run an inelastic, dynamic time history analysis. The Ruaumoko model consisted of two frame elements representing the pile and the column. The properties for the column and the pile used as input for Ruaumoko are listed in Tables 5.8 and 5.9, respectively.

**Table 5.8 Column properties for Ruaumoko**

<b>Property</b>	<b>Value</b>
Elastic modulus	2.49 MN/cm <sup>2</sup>
Cross-sectional area	1.17 m <sup>2</sup>
Moment of inertia	0.151 m <sup>4</sup>
Bilinear factor	6.44E-03
Plastic hinge length	0.866 m
Yield surface	
Compression yield force	39.4 MN
Compression force at B	24.5 MN
Yield moment at B	7.11 MN·m
Yield moment at 2/3B	7.92 MN·m
Yield moment at 1/3B	7.29 MN·m
Yield moment at P=0	5.24 MN·m
Tension yield force	11.4 MN

For both the column and pile elements, a Takeda hysteresis rule was utilized, with  $\alpha$  equal to 0.4 and  $\beta$  equal to 0.1. An axial load of 1.29 MN was applied to the top of the column. The participating seismic weight was 4.83 MN, which corresponds to a mass of 492 Mg. The input record used in the Ruaumoko analysis was the mean pulse record scaled to 139 cm/s representing the mean plus one standard deviation.

**Table 5.9 Pile properties for Ruaumoko**

<b>Property</b>	<b>Value</b>
Elastic modulus	2.49 MN/cm <sup>2</sup>
Cross-sectional area	1.17 m <sup>2</sup>
Moment of inertia	0.141 m <sup>4</sup>
Bilinear factor	5.77E-03
Plastic hinge length	0.866 m
Yield surface	
Compression yield force	37.3 MN
Compression force at B	24.5 MN
Yield moment at B	6.24 MN·m
Yield moment at 2/3B	7.01 MN·m
Yield moment at 1/3B	6.27 MN·m
Yield moment at P=0	4.08 MN·m
Tension yield force	8.54 MN

To more accurately model the forces in the joint region, the curvature response at the top of the column was used to determine the displacement loading protocol, rather than using the displacement response directly. The curvature response of the column reached a peak of 0.0499 1/m 1.56 sec into the record followed by a curvature in the opposite direction of 0.00846 1/m at 2.46 sec. These curvatures were scaled by two in order to match the scale of the laboratory models. A yield curvature of 0.00606 1/m and a plastic hinge length of 36.3 cm was used to determine the correct displacements at the top of the specimen. The first peak displacement was 6.90 cm followed by a peak of 1.40 cm in the opposite direction. The remainder of the loading protocol was designed to match tests previously performed at UCSD on identical specimens. This allowed for comparisons to be made and the impact of the pulse on the structure to be evaluated. After the pulse, the loading sequence consisted of the following peak displacements:

0.31 cm, 0.62 cm, 0.93 cm, 1.24 cm, 1.71 cm, 2.57 cm, 3.42 cm, 5.13 cm, 6.84 cm, 10.26 cm, 13.68 cm, and 17.10 cm. The loading protocol for the dynamic tests is plotted in Figure 5.6 below. The pseudo-static tests followed the same peak displacements stopping at the peaks and at various points of interest during the test. Details of the T-joint testing can be found in Gibson (2001).

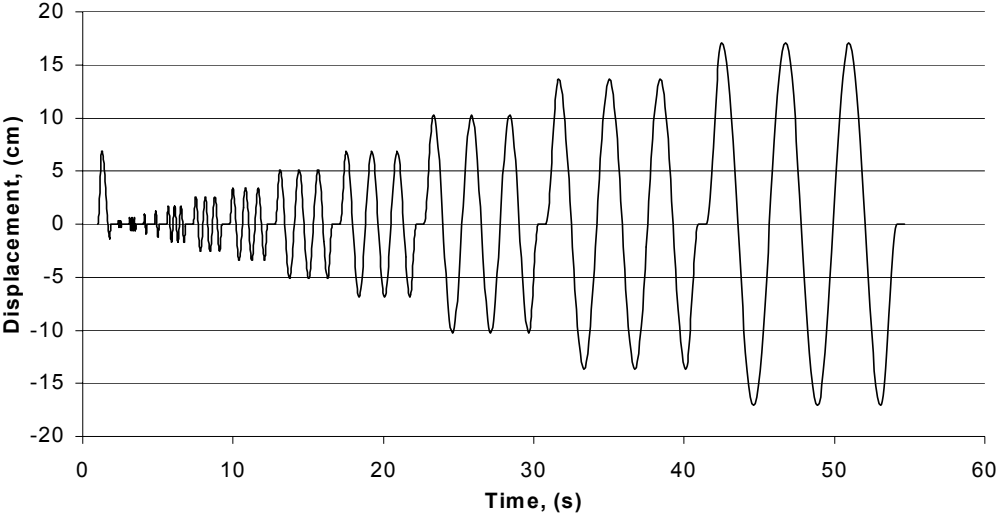


**Fig. 5.6 Loading protocol for the beam-column joint tests**

## 6 The Kocaeli and Chi-Chi Earthquakes

The Kocaeli, Turkey, earthquake on 17 August 1999, and the Chi-Chi, Taiwan, earthquake on 20 September 1999, added significantly to the records of the near-fault strong motion database. These earthquakes help to fill in aspects under-represented for large earthquakes. The Kocaeli earthquake matches in magnitude (7.4 moment magnitude) the Tabas, Iran, earthquake, which was the largest magnitude earthquake represented in the database. The Chi-Chi earthquake exceeds the Kocaeli earthquake with a 7.6 moment magnitude. These two earthquakes yielded a significant amount of data. In total, of the 21 records analyzed for the presence of a pulse, 9 were found to contain one. Curiously, these higher magnitude earthquakes did not demonstrate higher peak velocities. They did, however, have pulses of longer duration and period than the previous pulses analyzed. This effect is not because the records are at a greater distance from the fault. The maximum distance to fault rupture among these records is 8.7 km, whereas the maximum distance to the rupture surface before the addition of these records was 15.6 km. The minimum distance to the rupture surface in this set is 2.5 km, whereas the minimum distance to the rupture surface before the addition of these records was 0.2 km. The average distance to the rupture surface is essentially the same for both sets: 5.6 km for these records and 5.7 km for the earlier records.

The records found to contain a pulse are listed in Table 6.1.

**Table 6.1 Kocaeli and Chi-Chi records containing pulses**

Date	Quake	Moment Magnitude	Station	Direction	Peak Vel (cm/s)	Period (s)	
08/17/99	Kocaeli, Turkey	7.4	Yarimca Petkim <sup>1</sup>	FN	88	5.7	
09/20/99	Chi-Chi, Taiwan	7.6	CHY024 <sup>2</sup>	FN	62	4.0	
09/20/99	Chi-Chi, Taiwan	7.6	CHY028 <sup>2</sup>	FN	74	2.0	
09/20/99	Chi-Chi, Taiwan	7.6	CHY101 <sup>2</sup>	FN	82	4.6	
09/20/99	Chi-Chi, Taiwan	7.6	TCU076 <sup>2</sup>	FN	87	3.2	
09/20/99	Chi-Chi, Taiwan	7.6	TCU079 <sup>2</sup>	FN	68	0.7	
09/20/99	Chi-Chi, Taiwan	7.6	TCU129 <sup>2</sup>	FN	69	2.3	
09/20/99	Chi-Chi, Taiwan	7.6	WGK <sup>2</sup>	FN	72	3.3	
09/20/99	Chi-Chi, Taiwan	7.6	WNT <sup>2</sup>	FN	58	5.6	
					<b>Peak Vel</b>	<b>Period</b>	
					Maximum	88	5.7
					Minimum	58	0.7
					Mean	73	3.5
					Standard Deviation	10	1.7

Record sources: 1. Birgoren and Tarhan, 2000; 2. Lee et al., 1999.

The velocity time histories for all of these records are plotted in Figure 6.1. In this plot, the pulse is in bold. The isolated pulses are plotted together with the mean pulse in Figure 6.2. This figure is the same as Figure 4.2, with the addition of the pulses from the Kocaeli and Chi-Chi earthquakes. The resulting mean large velocity directivity pulse is plotted alone in Figure 6.3.

When this data are merged with the previous data, the resulting maximum and minimum peak velocities remain unaffected at 174 cm/s and 23 cm/s. The mean peak velocity is 89 cm/s with a standard deviation of 39 cm/s. The statistical data for the period of the combined data are: maximum = 9.3 s, minimum = 0.5 s, mean = 2.5 s, standard deviation = 1.8 s. The average number of cycles also remains unaffected at 1. The addition of this data changes the mean pulse insignificantly and serves to validate the data collected previously.

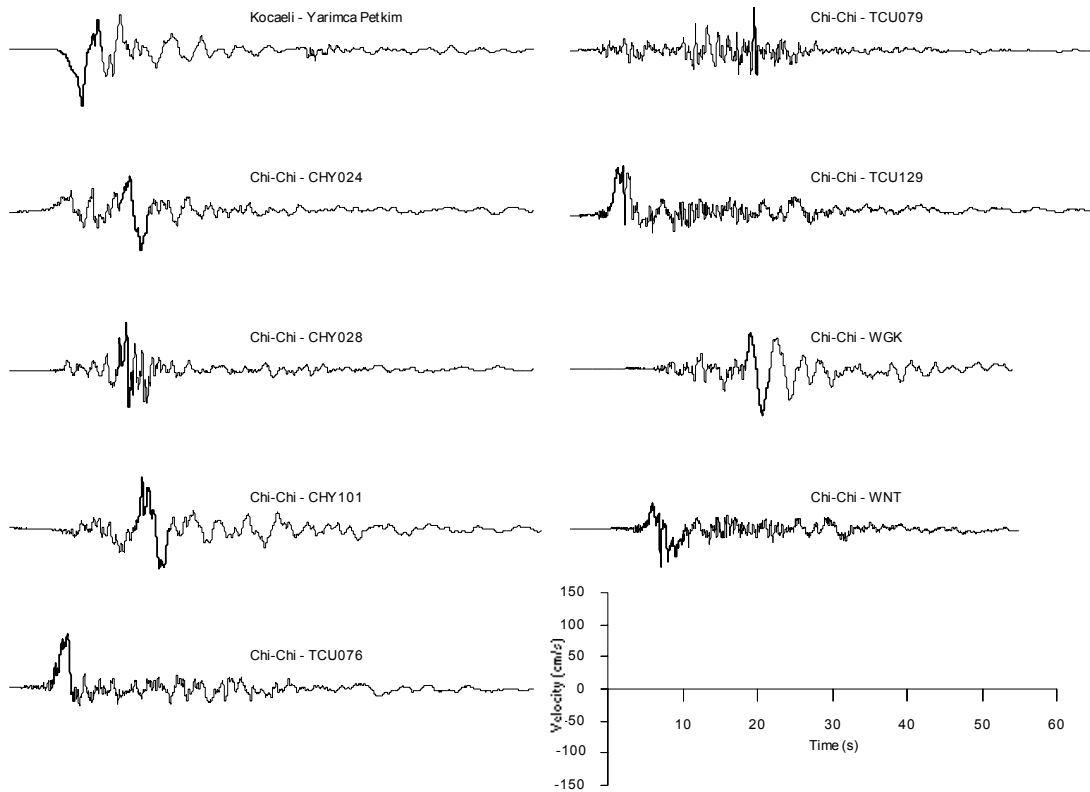


**Fig. 6.1 Kocaeli and Chi-Chi records found to contain a pulse. The pulse is in bold.**

The regression analysis to obtain attenuation relations presented in Section 3.5 is repeated here to include the data obtained from the Kocaeli and Chi-Chi earthquakes. For a definition of the geometric and seismological factors considered in this analysis, refer to Section 3.5. The correlation between these factors and the period and peak velocity is listed in Table 6.2. This analysis considers all the pulses considered in Section 3.5 and all the pulses from the Kocaeli and Chi-Chi earthquakes listed in Table 6.1.

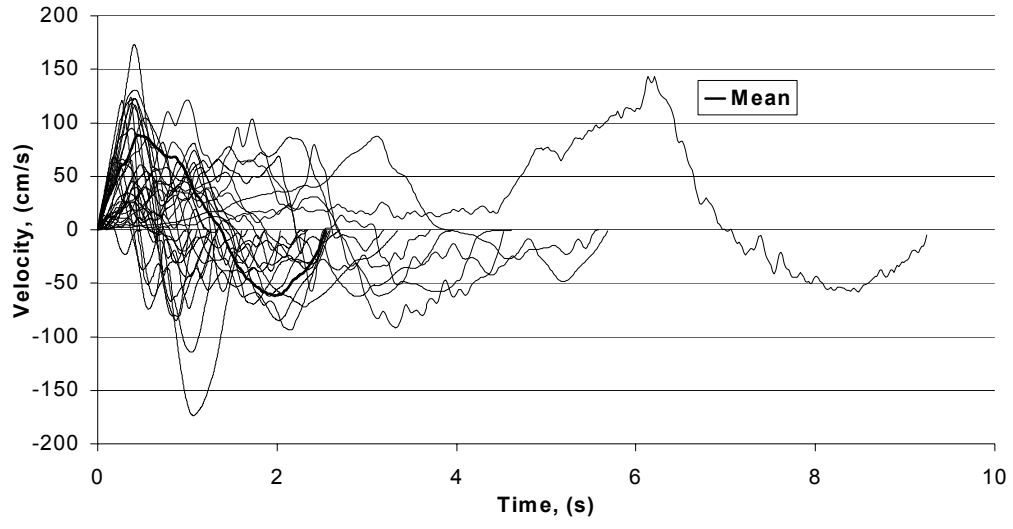


**Fig. 6.2 Isolated pulses and the mean pulse**

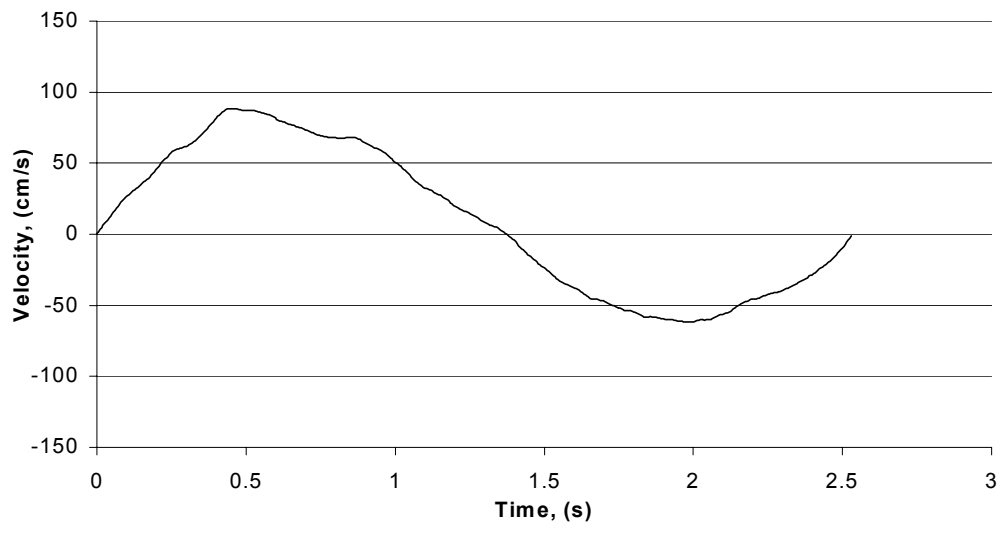


**Fig. 6.3 Mean pulse including the data from Kocaeli and Chi-Chi**

**Table 6.2 Correlation values for period and peak velocity**

	Period	Log(Period)	Peak Vel	Log(Peak Vel)
<b>M<sub>w</sub></b>	0.5202	0.5678	-0.0708	0.0816
<b>r</b>	-0.1105	-0.1774	-0.2493	-0.2480
<b>X</b>	-0.4056	-0.2727	0.1527	0.1099
<b>φ</b>	-0.4589	-0.5658	-0.1585	-0.2156
<b>Log(M<sub>w</sub>)</b>	0.5210	0.5718	-0.0580	0.0931
<b>Log(r)</b>	0.0257	-0.0154	-0.1486	-0.0976
<b>X cos(φ)</b>	-0.3607	-0.2168	0.1762	0.1412

These correlation values indicate that there is some weak relationship between the log of the period and the directivity angle and the log of the magnitude. The strongest correlation for the peak velocity is found between the log of the peak velocity and the distance to fault rupture and the directivity angle; however this correlation is very weak.

Regression on the log of the moment magnitude and the directivity angle to obtain the log of the period yielded an  $R^2$  value of 0.513. Analysis of the residuals from this regression shows two excessively high residuals. The analysis was repeated with the exclusion of the data from these outliers. The results from this regression demonstrate a slightly improved  $R^2$  value of 0.526. The coefficients resulting from this regression analysis are presented in equation form:

$$\text{Log}(\text{Period}) = -2.136 - 0.01020 \cdot \phi + 3.053 \cdot \text{Log}(M_w)$$

The fit of this equation to the data is demonstrated in Figures 6.4 and 6.5.

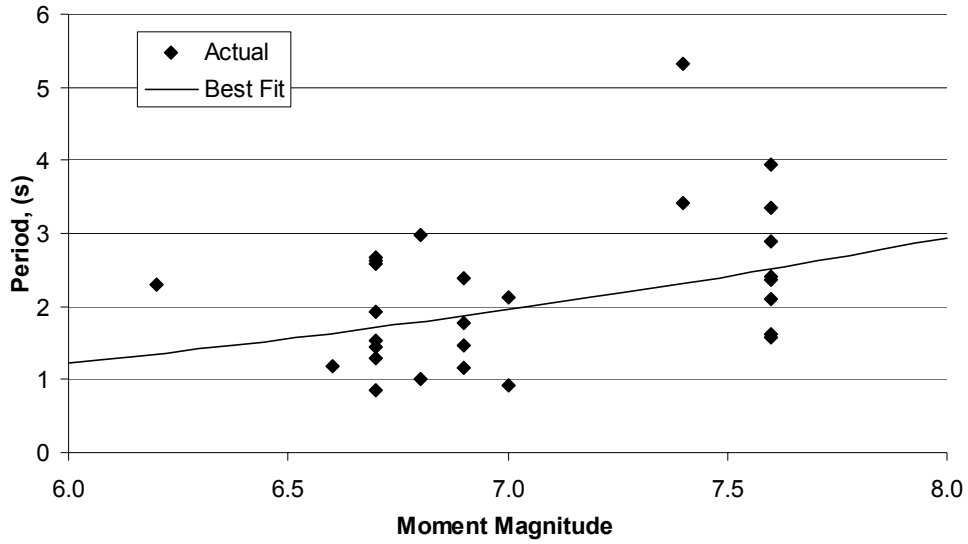


**Fig. 6.4** Period of the pulse predicted by  $M_w$ . Data are normalized to  $\phi = 15^\circ$ .

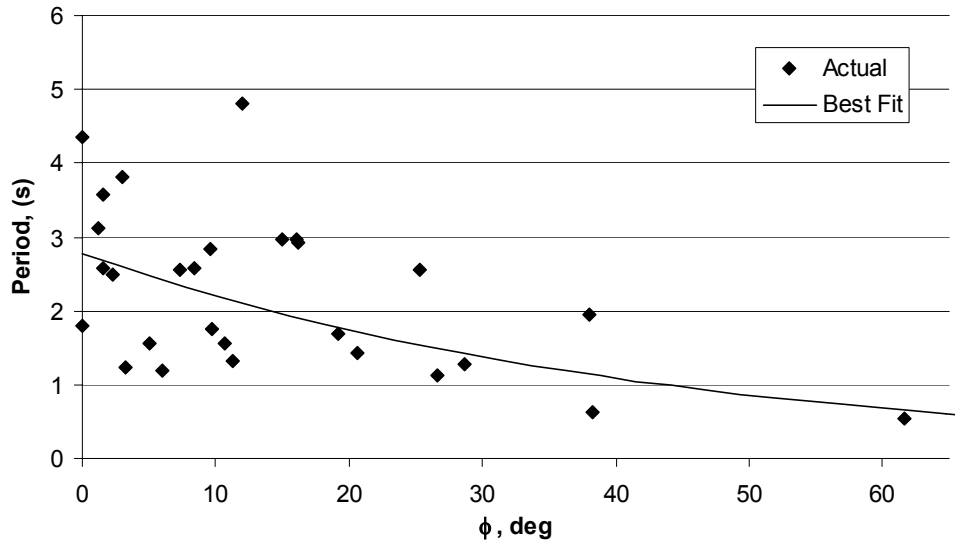


**Fig. 6.5** Period of the pulse predicted by  $\phi$ . Data are normalized to  $M_w = 7$ .

Regression of the distance to rupture surface and the directivity angle to obtain the log of the peak velocity resulted in a low  $R^2$  value of 0.098. Again, the residuals indicate two strong

outliers. These outliers were removed and the analysis was performed again. The new results give a slightly improved  $R^2$  value of 0.210. The coefficients from this analysis are given below:

$$\text{Log}(PV) = 2.123 - 0.03024 \cdot r - 0.002975 \cdot \phi$$

The fit of this equation to the actual data is illustrated in Figures 6.6 and 6.7.

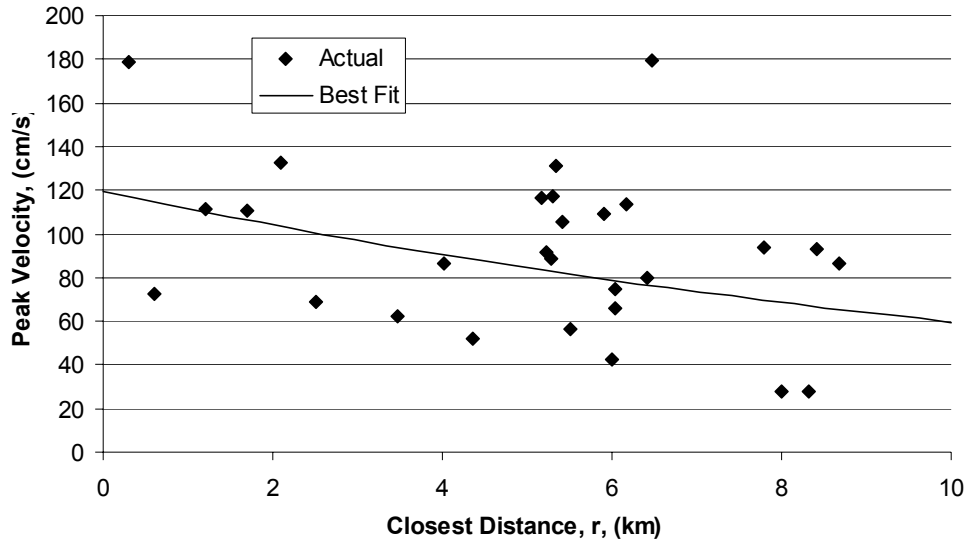


**Fig. 6.6** Peak velocity predicted by r. Data are normalized to  $\phi = 15^\circ$ .

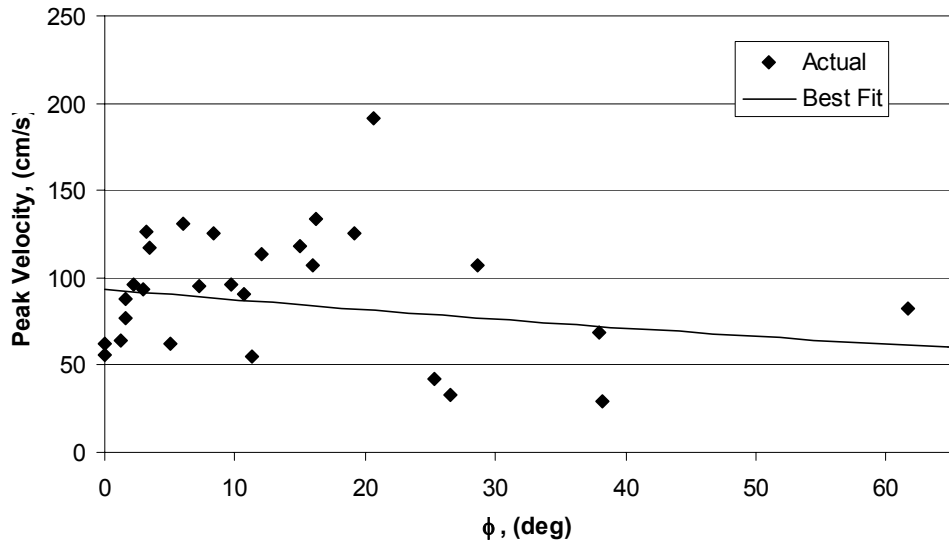


**Fig. 6.7** Peak velocity predicted by  $\phi$ . Data are normalized to r = 5 km.

The dependence of the period and the peak velocity of the pulse on the directivity angle,  $\phi$ , was not expected in this form from the current literature on directivity effects. It was expected that the effect of the directivity angle on the pulse would be coupled with the directivity ratio and have the form:

$$x \cos(\phi)$$

The sign of the  $\phi$  coefficient in the period attenuation relationship was also unexpected. It was expected that an increase in  $\phi$  would cause the pulse to lengthen in period and diminish in amplitude. The dependence of period on magnitude was expected. The dependence of peak velocity on the distance,  $r$ , was also expected; however, it was expected to be multiplied by the cosine of the directivity angle.

## 7 Summary and Conclusions

A large velocity directivity pulse occurs when the conditions of forward directivity are met. These conditions include:

1. The earthquake is sufficiently large (moment magnitude greater than 6);
2. The site is located sufficiently close to the fault rupture (within 10 km); and
3. The rupture propagates toward the site.

This large velocity directivity pulse will be evident in the fault-normal direction. It is typically located toward the front of the time history and consists of, on average, one cycle of motion. Peak velocities can range from 23 cm/sec to 174 cm/s with a mean value of 89 cm/sec. The period of the pulse can range from 0.5 sec to 9.3 sec with a mean value of 2.5 sec.

In defining the testing protocols, 24 near-fault time histories containing large velocity pulses were analyzed, and the pulses extracted from the record. The defining characteristics of the pulses (peak velocity and period) were averaged and an average pulse was constructed. This average pulse consisted of 1 full cycle of velocity motion, exhibited over a period of 2.2 sec and a peak velocity of 94 cm/sec. This pulse definition has been used to determine the loading protocol for over 9 specimens at three different universities.

For testing of the three column specimens the average pulse was used as the input motion in a single-degree-of-freedom, nonlinear program (NONLIN) to determine the response of the prototype bridge column to the average near-fault large velocity pulse. The response of the column was simplified and scaled. A standard cyclic loading sequence was then added after the pulse. The loading time histories for these tests are plotted in Figures 5.4 and 5.5. For testing of the four beam-column joint connections, a pulse demonstrating a peak velocity equal to the mean plus one standard deviation was used as input to a Ruaumoko model of the prototype structure. The curvature response of the structure was determined and scaled by two. A cyclic loading sequence was added to the pulse response.

Two of the specimens were loaded with a displacement time history as shown in Figure 5.6. The remaining two specimens were loaded following a pseudo-static regime with the same peak displacements and in the same order.

The inclusion of data from the Kocaeli and Chi-Chi earthquakes to the work already completed serves to confirm the accuracy of the database. The most significant change to the mean pulse with the inclusion of this data is an increase in the period of the pulse. The standard deviation of the peak velocities in the database is also slightly more restricted with the inclusion of the recent data.

## REFERENCES

- Abrahamson, N. (1998) "Seismological Aspects of Near-Fault Ground Motions." *5<sup>th</sup> Caltrans Seismic Research Workshop*, Sacramento, California, June
- Applied Technology Council (ATC) (1996) "Improved Seismic Design Criteria for California Bridges: Provisional Recommendations", ATC-32 Report, Palo Alto, California
- Attalla, M. R., Paret, T. F., and Freeman, S. A. (1998) "Near-source Behavior of Buildings Under Pulse-type Earthquakes." *Proceedings of the sixth US National Conference on Earthquake Engineering*, Seattle WA
- Bertero, V. V., Mahin, S. A., and Herrera, R. A. (1978) "A Seismic Design Implication of Near-fault San Fernando Earthquake Records." *Earthquake Engineering and Structural Dynamics*, Vol. 6, 31-34
- Birgoren, G., and Tarhan, C. (2000) "Kocaeli Earthquake-TURKEY." <http://www.koeri.boun.edu.tr/earthqk/earthquake.htm>, Kandalli Observatory and Earthquake Research Institute, Boğaziçi University, Data retrieved August
- Carr, A.J. (1998) "Ruaumoko – Program for Inelastic Dynamic Analysis." Department of Civil Engineering, University of Canterbury
- Charney, F. A. (1997) "NONLIN Version 5.50" Advanced Structural Concepts, Golden, Colorado
- Gibson, N. (2001) "The Effect of Large Velocity Pulses on Bridge Joints." Report presented to the University of California at San Diego, La Jolla, CA in partial satisfaction of the requirements for the degree Master of Science
- Hall, J. F., and Aagaard, B. T. (1998) "Fundamentals of the Near-Source Problem." *5<sup>th</sup> Caltrans Seismic Research Workshop*, Sacramento, California, June
- Hall, J. F., Heaton, T. H., Halling, M. W., and Wald, D. J. (1995) "Near-Source Ground Motion and its Effects on Flexible Buildings." *Earthquake Spectra*. Vol. 11, No. 4, November, 569-605
- Institute for Crustal Studies (ICS) (1999) "SMDB: The Strong Motion DataBase" <http://smdb.crustal.ucsb.edu/>, University of California, Santa Barbara, Data retrieved January
- Lee, W. H. K., Shin, T. C., Kuo, K. W., and Chen, K. C. (1999) "CWB Free-Field Strong-Motion Data from the 921 Chi-Chi Earthquake: Volume 1. Digital Acceleration Files on CD-ROM." Pre-Publication Version (December 6, 1999), Seismology Center, Central Weather Bureau, Taipei, Taiwan
- Mahin, S., and Hachem, M. (1998) "Response of Simple Bridge Structures to Near-Fault Ground Motions." *5<sup>th</sup> Caltrans Seismic Research Workshop*, Sacramento, California, June

- Makley, B. (2001) "Seismic Behavior of Bridge Shear Columns Subjected to Near Field Pulse Loading." Report presented to the University of California at San Diego, La Jolla, CA in partial satisfaction of the requirements for the degree Master of Science
- Mayes, R. L., and Shaw, A. (1997) "The Effects of Near Fault Ground Motions on Bridge Columns." *Proceedings of the FHWA/NCEER Workshop on the National Representation of Seismic Ground Motion for New and Existing Highway Facilities*. Burlingame, California, May 29-30, 319-340
- Orozco, G.L. (2001) "The Effect of Large Velocity Pulses on Bridge Piers." Report presented to the University of California at San Diego, La Jolla, CA in partial satisfaction of the requirements for the degree Master of Science
- Parsi, M (1998) "Strong motion Database System." [http://www.ldeo.columbia.edu/cgi-bin/strongmo-cgi-bin/smdb\\_startStrongmo.pl](http://www.ldeo.columbia.edu/cgi-bin/strongmo-cgi-bin/smdb_startStrongmo.pl), Lamont-Doherty Earth Observatory, Columbia University, Data retrieved November
- Silva, W. (1998) "PEER Strong Motion Catalog." July
- Somerville, P. (1998) "Suites of Earthquake Ground Motions for Analysis of Steel Moment Frame Structures." [http://quiver.eerc.berkeley.edu:8080/studies/system/ground\\_motions.html](http://quiver.eerc.berkeley.edu:8080/studies/system/ground_motions.html) SAC Joint Venture, Data Retrieved November
- Somerville, P. (1997) "The Characteristics and Quantification of Near Fault Ground Motion." *Proceedings of the FHWA/NCEER Workshop on the National Representation of Seismic Ground Motion for New and Existing Highway Facilities*. Burlingame, California, May 29-30, 293-318
- Somerville, P., and Graves, R. (1993) "Conditions that Give Rise to Unusually Large Long Period Ground Motions." *The structural design of tall buildings*. Vol. 2, 211-232

## PEER REPORTS

PEER reports are available from the National Information Service for Earthquake Engineering (NISEE). To order PEER reports, please contact the Pacific Earthquake Engineering Research Center, 1301 South 46<sup>th</sup> Street, Richmond, California 94804-4698. Tel.: (510) 231-9468; Fax: (510) 231-9461.

- PEER 2002/23**     *Effects of Large Velocity Pulses on Reinforced Concrete Bridge Columns.* Greg L. Orozco and Scott A. Ashford. April 2002.
- PEER 2002/22**     *Characterization of Large Velocity Pulses for Laboratory Testing.* Kenneth E. Cox and Scott A. Ashford. April 2002.
- PEER 2002/21**     *Fourth U.S.-Japan Workshop on Performance-Based Earthquake Engineering Methodology for Reinforced Concrete Building Structures.* December 2002.
- PEER 2002/20**     *Barriers to Adoption and Implementation of PBEE Innovations.* Peter J. May. August 2002.
- PEER 2002/19**     *Economic-Engineered Integrated Models for Earthquakes: Socioeconomic Impacts.* Peter Gordon, James E. Moore II, and Harry W. Richardson. July 2002.
- PEER 2002/18**     *Assessment of Reinforced Concrete Building Exterior Joints with Substandard Details.* Chris P. Pantelides, Jon Hansen, Justin Nadauld, and Lawrence D. Reaveley. May 2002.
- PEER 2002/17**     *Structural Characterization and Seismic Response Analysis of a Highway Overcrossing Equipped with Elastomeric Bearings and Fluid Dampers: A Case Study.* Nicos Makris and Jian Zhang. November 2002.
- PEER 2002/16**     *Estimation of Uncertainty in Geotechnical Properties for Performance-Based Earthquake Engineering.* Allen L. Jones, Steven L. Kramer, and Pedro Arduino. December 2002.
- PEER 2002/15**     *Seismic Behavior of Bridge Columns Subjected to Various Loading Patterns.* Asadollah Esmaeily-Gh. and Yan Xiao. December 2002.
- PEER 2002/14**     *Inelastic Seismic Response of Extended Pile Shaft Supported Bridge Structures.* T.C. Hutchinson, R.W. Boulanger, Y.H. Chai, and I.M. Idriss. December 2002.
- PEER 2002/13**     *Probabilistic Models and Fragility Estimates for Bridge Components and Systems.* Paolo Gardoni, Armen Der Kiureghian, and Khalid M. Mosalam. June 2002.
- PEER 2002/12**     *Effects of Fault Dip and Slip Rake on Near-Source Ground Motions: Why Chi-Chi Was a Relatively Mild M7.6 Earthquake.* Brad T. Aagaard, John F. Hall, and Thomas H. Heaton. December 2002.
- PEER 2002/11**     *Analytical and Experimental Study of Fiber-Reinforced Strip Isolators.* James M. Kelly and Shakhzod M. Takhirov. September 2002.
- PEER 2002/10**     *Centrifuge Modeling of Settlement and Lateral Spreading with Comparisons to Numerical Analyses.* Sivapalan Gajan and Bruce L. Kutter. January 2003.

- PEER 2002/09**      *Documentation and Analysis of Field Case Histories of Seismic Compression during the 1994 Northridge, California, Earthquake.* Jonathan P. Stewart, Patrick M. Smith, Daniel H. Whang, and Jonathan D. Bray. October 2002.
- PEER 2002/08**      *Component Testing, Stability Analysis and Characterization of Buckling-Restrained Unbonded Braces<sup>TM</sup>.* Cameron Black, Nicos Makris, and Ian Aiken. September 2002.
- PEER 2002/07**      *Seismic Performance of Pile-Wharf Connections.* Charles W. Roeder, Robert Graff, Jennifer Soderstrom, and Jun Han Yoo. December 2001.
- PEER 2002/06**      *The Use of Benefit-Cost Analysis for Evaluation of Performance-Based Earthquake Engineering Decisions.* Richard O. Zerbe and Anthony Falit-Baiamonte. September 2001.
- PEER 2002/05**      *Guidelines, Specifications, and Seismic Performance Characterization of Nonstructural Building Components and Equipment.* André Filiatrault, Constantin Christopoulos, and Christopher Stearns. September 2001.
- PEER 2002/04**      *Consortium of Organizations for Strong-Motion Observation Systems and the Pacific Earthquake Engineering Research Center Lifelines Program: Invited Workshop on Archiving and Web Dissemination of Geotechnical Data, 4–5 October 2001.* September 2002.
- PEER 2002/03**      *Investigation of Sensitivity of Building Loss Estimates to Major Uncertain Variables for the Van Nuys Testbed.* Keith A. Porter, James L. Beck, and Rustem V. Shaikhutdinov. August 2002.
- PEER 2002/02**      *The Third U.S.-Japan Workshop on Performance-Based Earthquake Engineering Methodology for Reinforced Concrete Building Structures.* July 2002.
- PEER 2002/01**      *Nonstructural Loss Estimation: The UC Berkeley Case Study.* Mary C. Comerio and John C. Stallmeyer. December 2001.
- PEER 2001/16**      *Statistics of SDF-System Estimate of Roof Displacement for Pushover Analysis of Buildings.* Anil K. Chopra, Rakesh K. Goel, and Chatpan Chintanapakdee. December 2001.
- PEER 2001/15**      *Damage to Bridges during the 2001 Nisqually Earthquake.* R. Tyler Ranf, Marc O. Eberhard, and Michael P. Berry. November 2001.
- PEER 2001/14**      *Rocking Response of Equipment Anchored to a Base Foundation.* Nicos Makris and Cameron J. Black. September 2001.
- PEER 2001/13**      *Modeling Soil Liquefaction Hazards for Performance-Based Earthquake Engineering.* Steven L. Kramer and Ahmed-W. Elgamal. February 2001.
- PEER 2001/12**      *Development of Geotechnical Capabilities in OpenSees.* Boris Jeremic. September 2001.
- PEER 2001/11**      *Analytical and Experimental Study of Fiber-Reinforced Elastomeric Isolators.* James M. Kelly and Shakhzod M. Takhirov. September 2001.
- PEER 2001/10**      *Amplification Factors for Spectral Acceleration in Active Regions.* Jonathan P. Stewart, Andrew H. Liu, Yoojoong Choi, and Mehmet B. Baturay. December 2001.

- PEER 2001/09** *Ground Motion Evaluation Procedures for Performance-Based Design.* Jonathan P. Stewart, Shyh-Jeng Chiou, Jonathan D. Bray, Robert W. Graves, Paul G. Somerville, and Norman A. Abrahamson. September 2001.
- PEER 2001/08** *Experimental and Computational Evaluation of Reinforced Concrete Bridge Beam-Column Connections for Seismic Performance.* Clay J. Naito, Jack P. Moehle, and Khalid M. Mosalam. November 2001.
- PEER 2001/07** *The Rocking Spectrum and the Shortcomings of Design Guidelines.* Nicos Makris and Dimitrios Konstantinidis. August 2001.
- PEER 2001/06** *Development of an Electrical Substation Equipment Performance Database for Evaluation of Equipment Fragilities.* Thalia Agnanos. April 1999.
- PEER 2001/05** *Stiffness Analysis of Fiber-Reinforced Elastomeric Isolators.* Hsiang-Chuan Tsai and James M. Kelly. May 2001.
- PEER 2001/04** *Organizational and Societal Considerations for Performance-Based Earthquake Engineering.* Peter J. May. April 2001.
- PEER 2001/03** *A Modal Pushover Analysis Procedure to Estimate Seismic Demands for Buildings: Theory and Preliminary Evaluation.* Anil K. Chopra and Rakesh K. Goel. January 2001.
- PEER 2001/02** *Seismic Response Analysis of Highway Overcrossings Including Soil-Structure Interaction.* Jian Zhang and Nicos Makris. March 2001.
- PEER 2001/01** *Experimental Study of Large Seismic Steel Beam-to-Column Connections.* Egor P. Popov and Shakhzod M. Takhirov. November 2000.
- PEER 2000/10** *The Second U.S.-Japan Workshop on Performance-Based Earthquake Engineering Methodology for Reinforced Concrete Building Structures.* March 2000.
- PEER 2000/09** *Structural Engineering Reconnaissance of the August 17, 1999 Earthquake: Kocaeli (Izmit), Turkey.* Halil Sezen, Kenneth J. Elwood, Andrew S. Whittaker, Khalid Mosalam, John J. Wallace, and John F. Stanton. December 2000.
- PEER 2000/08** *Behavior of Reinforced Concrete Bridge Columns Having Varying Aspect Ratios and Varying Lengths of Confinement.* Anthony J. Calderone, Dawn E. Lehman, and Jack P. Moehle. January 2001.
- PEER 2000/07** *Cover-Plate and Flange-Plate Reinforced Steel Moment-Resisting Connections.* Taejin Kim, Andrew S. Whittaker, Amir S. Gilani, Vitelmo V. Bertero, and Shakhzod M. Takhirov. September 2000.
- PEER 2000/06** *Seismic Evaluation and Analysis of 230-kV Disconnect Switches.* Amir S. J. Gilani, Andrew S. Whittaker, Gregory L. Fenves, Chun-Hao Chen, Henry Ho, and Eric Fujisaki. July 2000.
- PEER 2000/05** *Performance-Based Evaluation of Exterior Reinforced Concrete Building Joints for Seismic Excitation.* Chandra Clyde, Chris P. Pantelides, and Lawrence D. Reaveley. July 2000.
- PEER 2000/04** *An Evaluation of Seismic Energy Demand: An Attenuation Approach.* Chung-Che Chou and Chia-Ming Uang. July 1999.

- PEER 2000/03** *Framing Earthquake Retrofitting Decisions: The Case of Hillside Homes in Los Angeles.* Detlof von Winterfeldt, Nels Roselund, and Alicia Kitsuse. March 2000.
- PEER 2000/02** *U.S.-Japan Workshop on the Effects of Near-Field Earthquake Shaking.* Andrew Whittaker, ed. July 2000.
- PEER 2000/01** *Further Studies on Seismic Interaction in Interconnected Electrical Substation Equipment.* Armen Der Kiureghian, Kee-Jeung Hong, and Jerome L. Sackman. November 1999.
- PEER 1999/14** *Seismic Evaluation and Retrofit of 230-kV Porcelain Transformer Bushings.* Amir S. Gilani, Andrew S. Whittaker, Gregory L. Fenves, and Eric Fujisaki. December 1999.
- PEER 1999/13** *Building Vulnerability Studies: Modeling and Evaluation of Tilt-up and Steel Reinforced Concrete Buildings.* John W. Wallace, Jonathan P. Stewart, and Andrew S. Whittaker, editors. December 1999.
- PEER 1999/12** *Rehabilitation of Nonductile RC Frame Building Using Encasement Plates and Energy-Dissipating Devices.* Mehrdad Sasani, Vitelmo V. Bertero, James C. Anderson. December 1999.
- PEER 1999/11** *Performance Evaluation Database for Concrete Bridge Components and Systems under Simulated Seismic Loads.* Yael D. Hose and Frieder Seible. November 1999.
- PEER 1999/10** *U.S.-Japan Workshop on Performance-Based Earthquake Engineering Methodology for Reinforced Concrete Building Structures.* December 1999.
- PEER 1999/09** *Performance Improvement of Long Period Building Structures Subjected to Severe Pulse-Type Ground Motions.* James C. Anderson, Vitelmo V. Bertero, and Raul Bertero. October 1999.
- PEER 1999/08** *Envelopes for Seismic Response Vectors.* Charles Menun and Armen Der Kiureghian. July 1999.
- PEER 1999/07** *Documentation of Strengths and Weaknesses of Current Computer Analysis Methods for Seismic Performance of Reinforced Concrete Members.* William F. Cofer. November 1999.
- PEER 1999/06** *Rocking Response and Overturning of Anchored Equipment under Seismic Excitations.* Nicos Makris and Jian Zhang. November 1999.
- PEER 1999/05** *Seismic Evaluation of 550 kV Porcelain Transformer Bushings.* Amir S. Gilani, Andrew S. Whittaker, Gregory L. Fenves, and Eric Fujisaki. October 1999.
- PEER 1999/04** *Adoption and Enforcement of Earthquake Risk-Reduction Measures.* Peter J. May, Raymond J. Burby, T. Jens Feeley, and Robert Wood.
- PEER 1999/03** *Task 3 Characterization of Site Response General Site Categories.* Adrian Rodriguez-Marek, Jonathan D. Bray, and Norman Abrahamson. February 1999.
- PEER 1999/02** *Capacity-Demand-Diagram Methods for Estimating Seismic Deformation of Inelastic Structures: SDF Systems.* Anil K. Chopra and Rakesh Goel. April 1999.

- PEER 1999/01** *Interaction in Interconnected Electrical Substation Equipment Subjected to Earthquake Ground Motions.* Armen Der Kiureghian, Jerome L. Sackman, and Kee-Jeung Hong. February 1999.
- PEER 1998/08** *Behavior and Failure Analysis of a Multiple-Frame Highway Bridge in the 1994 Northridge Earthquake.* Gregory L. Fenves and Michael Ellery. December 1998.
- PEER 1998/07** *Empirical Evaluation of Inertial Soil-Structure Interaction Effects.* Jonathan P. Stewart, Raymond B. Seed, and Gregory L. Fenves. November 1998.
- PEER 1998/06** *Effect of Damping Mechanisms on the Response of Seismic Isolated Structures.* Nicos Makris and Shih-Po Chang. November 1998.
- PEER 1998/05** *Rocking Response and Overturning of Equipment under Horizontal Pulse-Type Motions.* Nicos Makris and Yiannis Roussos. October 1998.
- PEER 1998/04** *Pacific Earthquake Engineering Research Invitational Workshop Proceedings, May 14–15, 1998: Defining the Links between Planning, Policy Analysis, Economics and Earthquake Engineering.* Mary Comerio and Peter Gordon. September 1998.
- PEER 1998/03** *Repair/Upgrade Procedures for Welded Beam to Column Connections.* James C. Anderson and Xiaojing Duan. May 1998.
- PEER 1998/02** *Seismic Evaluation of 196 kV Porcelain Transformer Bushings.* Amir S. Gilani, Juan W. Chavez, Gregory L. Fenves, and Andrew S. Whittaker. May 1998.
- PEER 1998/01** *Seismic Performance of Well-Confined Concrete Bridge Columns.* Dawn E. Lehman and Jack P. Moehle. December 2000.